공학박사 학위논문

INTERFERENCE MITIGATION SCHEME FOR AUTOMOTIVE FMCW RADAR

정확한 목표물 검출을 위한 차량용 FMCW 레이더에서의 간섭 제거 기법

2016년 2월

서울대학교 대학원

전기·컴퓨터 공학부

최정환

Abstract

INTERFERENCE MITIGATION SCHEME FOR AUTOMOTIVE FMCW RADAR

Junghwan Choi
Department of Electrical Engineering and computer science
The Graduate School
Seoul National University

As the number of vehicles on the road is increased, the incidence of traffic accident is gradually increased and the number of death is also increased. Most accidents are due to carelessness of the driver. If the vehicle can actively recognize the dangerous situation and alert the driver to avoid accident, it will be a great help to the driver. Sensor technologies have been developed by many car manufacturers and automobile device companies. There are many sensor used in vehicles, such as camera, LIDAR, radar and ultrasonic wave. Among these sensors, radar sensor is key device for adaptive cruise control (ACC), because it provides superior penetration capability through any type of weather condition, and can be used in the day or night. Meanwhile, camera cannot be used in the night or under rainy condition. LIDAR is still expensive

to commercialize. Ultrasonic wave is used in very short range.

There are several types of radar sensor, such as pulse doppler radar, stepped frequency pulse doppler (SFPD) radar, frequency modulated continuous wave (FMCW) radar and random noise radar. While pulse doppler radar and random noise radar need high-performance hardware for digital processing and SFPD radar needs additional processing, FMCW radar is widely used for automotive radar due to its easy implementation and high resolution. Linearly modulated chirp signal, such as triangular or trapezoidal signal, is used in FMCW radar.

With an increasing number of automotive radar, radar may receive signals from other radars as well as targets. In order to prevent radar malfunction, the effect of the interference should be removed. The techniques to mitigate the interference have been developed, such as pre-FFT processing for directly removing the interference or post-FFT processing for canceling the effect of interference.

In this dissertation, the effects of the interference between FMCW radars are analyzed. Narrow band interference, which results in the ghost target peak, is generated between identical radars or similar radars whose chirp slopes are slightly different. Mostly, wide band interference is generated and it increases the noise floor. Hence, we propose methods for removing the wide band interference. The shape of wide band interference is impulse-like signal, because its frequency lies on entire system bandwidth. The interference signals are suppressed in the time domain by using their envelope. This method is verified by simulation results and also measurement data in an

anechoic chamber.

In spite of suppressing the interference in the time domain, traces of the interference still remain in the mixer signals. For this reason, the desired angles of target are not estimated well. Since desired target signal is sum of sinusoids, the partial portion which the interference was suppressed is restored by using linear prediction. To predict the signal more correctly, the asymmetric window function is proposed and by using this function, forward and backward predicted signals are crossfaded asymmetrically. This method is also verified by simulation results.

Keywords : FMCW, Interference, Suppression, Linear prediction, AR model, Restoration

Student Number : 2010 - 30234

Contents

List of Tables

List of Figures

Chapter 1. Introduction

As the needs for automotive safety and convenience increase, various radar systems such as the pulse doppler radar [1], the noise radar [2], and the frequency-modulated continuous-wave (FMCW) radar [3]-[5] for guidance and collision avoidance are drawing increased attentions. Among these radar systems, the FMCW radar system, operating at 77 GHz, has been considered as an attractive solution due to its low costs, small size, and low transmission power requirement. Furthermore, the FMCW radar can estimate both the target distance and velocity simultaneously, and it can be easily equipped within automotive vehicles [6].

The aim of automotive radar is to guarantee safety of drivers and pedestrians form unexpected accident in various traffic situations. The system for this aim is called driver assistance system (DAS). Many automobile device companies have already developed many kinds of DASs such as adaptive cruise control (ACC), forward collision warning (FCW), pre-crash safety (PCS), blind spot detection (BSD), lane change assist (LCA) and rear cross traffic alert application (RCTA) system. ACC system is a radar-based system that can detect the vehicles in front, and adjust speed of the vehicles to keep a pre-set following distance, even under fog and rain conditions. FCW system is in-vehicle electronic that monitor the roadway in front of the host vehicle and warn the driver when a potential collision risk exists. When the sign of collision is detected, it provides a red light that flashes on the windshield. PCS

is system that detects the potential collision using the sensor and activates all necessary component such as brakes, airbag or steering in the car to avoid an accident. The vehicles on adjacent lanes can be avoided by BSD system which is invisibly mounted in the corners of the rear bumper. Also, the field of view for LCA system is selected to cover most of the blind spot warning zone and area containing neighbor lanes. An acoustic warning for drivers from BSD sensor would be helpful in a critical situation. RCTA system can assist drivers in backing up by warning drivers of impending traffic while reversing.

As the number of vehicles with automotive radar systems increases, mutual interference has become a crucial issue [7]-[9]. Mutual interference is caused by sharing the same or a part of the frequency bands with other automotive radar systems. Interference signals between FMCW radar systems lead to the generation of ghost target peaks as well as the increase of noise floor level in the frequency domain. In such situations, the radar system might fail to detect targets or may return incorrect target information due to low signal-to-noise ratio (SNR).

A variety of interference mitigation techniques have been proposed for automotive radar systems, which help to estimate accurate target information. Almost all automotive radars use the linear polarization. It can be concluded that by using cross polarized orientation degree between the polarization direction of the interferer antenna and the victim antenna, a decoupling typically more than 20 dB can be achieved [10]. The decoupling effect depends on the specific antenna parameter. Interference mitigation techniques in the frequency domain consist of measures which avoid that other radars

transmit in the reception bandwidth of a given radar. To achieve this, the reception bandwidth of the victim radar and the transmission bandwidths of the interferer radars need to be shifted in order to separate them in the frequency domain. In [11], a pre-crash radar sensor using a spread spectrum technique involving a long pseudo-noise sequence was presented, which requires a high data rate and returns low-resolution results. A coded stepped-FMCW signal for automotive radar applications in [12] provides a high resolution and multiple target detection capability as well as a good anti-interference capability, whereas its signal processing steps require huge computational complexity compared to the conventional FMCW radar system. The signal processing methods, such as pre-fast-Fourier transform (FFT) and post-FFT, were suggested to minimize the interference effect [7], [13]. However, these approaches are known to be ineffective in some circumstances in which the sweep time differences between mutually interfering FMCW radars are short. In [14], the effect of interference was reduced by using Prony modelling. To enhance the anti-interference capability of the conventional FMCW radar, a Pseudo Noise (PN)-modulated FMCW radar signal is used in [15] and an automotive radar for short range based on ultra-wideband (UWB) technology is studied in [16]. To avoid the interference between different users, the radar based on transmitting periodically pseudo random codes. A random timing of the time domain modulation of transmit frequency is attempted; for example, various pause lengths before the next FMCW chirp starts can be used or various FMCW slopes can be used [17]. In the space domain, mechanically or electronically scanned beam can be used to reduce

interference risk. By choosing the scanned azimuth or elevation range adaptive to the current environment.

In this dissertation, we propose a novel interference suppression scheme for interference-limited FMCW radar systems. The scheme uses a unique behavior of mutual interference in the time domain to detect the interference components. Clipping and weighted-envelope normalization are suggested as a measure of deciding whether the time sample of the signal is a mutual interference. The proposed algorithm minimizes the effect of the interference by suppressing the detected interference signal. It suppresses the interference signal by a simple post-processing technique. Thus proposed algorithm is compatible with an existing FMCW radar system, while the conventional approaches [11]-[12], [15] have to create new types of transmitting signals. Since, most interference signals can be detected and suppressed regardless of the interference strength, there is no reduction in performance of detecting targets in the high signal-to-interference ratio (SIR).

Because that the interference signals and target signals are not separated perfectly, the effect of the interference still remain after suppressing the interference. It leads to estimate incorrect angles of targets. Therefore, the method for replacing the part of distortion with new predicted signal is proposed. The restoration method is carried out by using linear prediction [18]-[21]. Since the mixer signal is composed of the sum of M sinusoids, it can be expressed by at least $2M$ order linear combination [22]. Also, in order to correct prediction, the asymmetric window function is proposed. The predicted signal by using linear prediction with asymmetric window enables

to correctly estimate angles of targets.

The remainder of this dissertation is organized as follows. In Chapter 2, analysis of technologies in automotive FMCW radar and system design of automotive FMCW radar are presented. In the section 2 of Chapter 2, the fundamental equation of radar is analyzed. In the section 3 of Chapter 2, the mathematical model for automotive FMCW radar is presented. In the section 4 of Chapter 2, overall signal processing for detecting targets in automotive FMCW radar is presented. In the section 5 of Chapter 2, system design of FMCW radar waveform is presented. In the section 6 of Chapter 2, analysis of CFAR algorithm for detecting targets is presented. In Chapter 3, analysis of the interference between automotive FMCW radars is presented. In the section 2 of Chapter 3, the fundamental equation of radar with interference is presented. In the section 3 of Chapter 3, the mathematical model for automotive radar with interference is presented. In the section 4 of Chapter 3, the interference between FMCW radar classified and the effect of the interference is analyzed including simulation results. In Chapter 4, the algorithm of mitigating the interference between FMCW radar and the method for restoring the signal are proposed. In the section 2 and the section 3 of Chapter 4, the algorithm using direct suppression method and the restoration method using linear prediction are proposed and the effect of the proposed algorithm is exploited with simulation result and experiment result, respectively. Finally, the conclusion follows in the section 4 of Chapter 4.

Chapter 2. FMCW RADAR Principles

2.1 Introduction

In this chapter, FMCW radar system widely used for automotive radar is introduced. The FMCW radar has been considered by Axelsson [23] by applying to the specular point theory [24]. In order to estimate range, it is considered in [25] FMCW architectures which rely on coherent processing of the harmonics in the post-mixing spectrum.

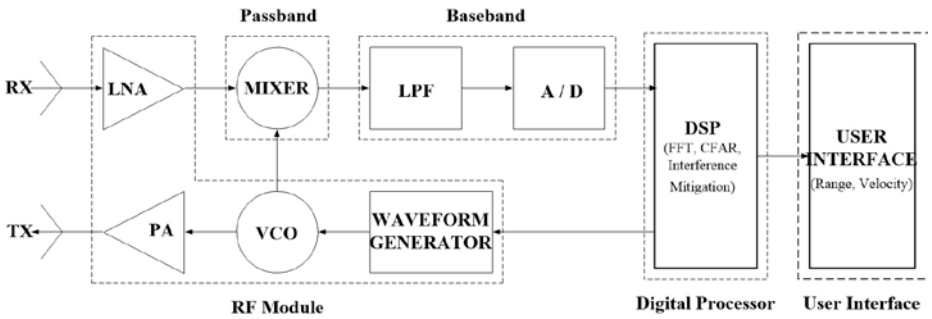

Figure 2.1 Schematic diagram of FMCW radar

A typical FMCW radar system is presented in Figure 2.1. A chirp signal modulated by the waveform generator is generated using a voltage-controlled oscillator (VCO). The amplified signal is transmitted into the air and the reflected signal from the target is received with a time delay and Doppler frequency shift. The beat frequency caused by the frequency shift of the

received signal is detected in the mixer.

The specification of typical FMCW radar is shown in Table 2.1.

Table 2.1 The specification of typical FMCW radar

Item	**Specification**
Frequency	76 ~ 77GHz
Transmitted power	< 10 mW
Range	0 ~ 240 m
Range resolution	< 1 m
Relative speed	-180 ~ 360 km/h
Speed resolution	< 1 km/h
Detection angle	±45° (SRR) / ±10° (LRR)
Angle estimation	< 1°
Multiple target detection	Yes
Frame rate	< 100 ms

Also, the techniques used for estimating the location of targets in the FMCW radar are analyzed in this chapter. In the section 2 and 3, the mathematical model for FMCW signal are discussed. The method for computing range and velocity of target from the estimated beat frequency and the method for peak detection from spectrum in the frequency domain are analyzed in section 5 and 6, respectively. In the last chapter, the method for estimating angle of target is analyzed.

2.2 Radar Equation

Radar equation is a basic theory for radar system. The equation represents the dependences of the transmitted power P_t, the target range R, the radar antenna gain G, the radar cross section (RCS) σ and wavelength of carrier frequency λ. The radar equation for received power is defined as follows.

$$P_r = \frac{P_t G_t \sigma}{\left(4\pi R^2\right)^2} A_e = \frac{P_t G_t G_r \lambda^2 \sigma}{\left(4\pi\right)^3 R^4} \tag{2.1}$$

From the equation, maximum target range can be theoretically determined by given radar specification. Equation can be converted to decibel levels as follows.

$$P_r = P_t + 10\log\left(\frac{\lambda^2}{\left(4\pi\right)^3}\right) + G_t + G_r + \sigma - 40\log\left(R\right) - 2\alpha R_{km} \tag{2.2}$$

where α is the atmospheric attenuation.

The noise floor is defined as follows.

$$N_{dBm} = 10\log\left(kT\beta\right) + NF + 30 \tag{2.3}$$

where k is the Boltzmann's constant (1.38×10^{-23} J/K), T is the absolute temperature (300K), β is the receiver bandwidth and NF is the receiver

noise figure.

The received power with RCS of 1 m^2 at various ranges and weather conditions is shown in Figure. The noise floor for typical FMCW radar can be obtained from (2.3) and value is -128dBm.

Assuming a Swerling type 2 target, a detection probability P_d is 0.95 and a false alarm probability P_{fa} is 10^{-6}, the required signal-to-noise (SNR) is 24.1 dB [26]. From Figure 2.2, the SNR at 200m for atmospheric attenuation of 20 mm/h is greater than 25 dB and so detection of target which is up to 200 m is sufficiently guaranteed.

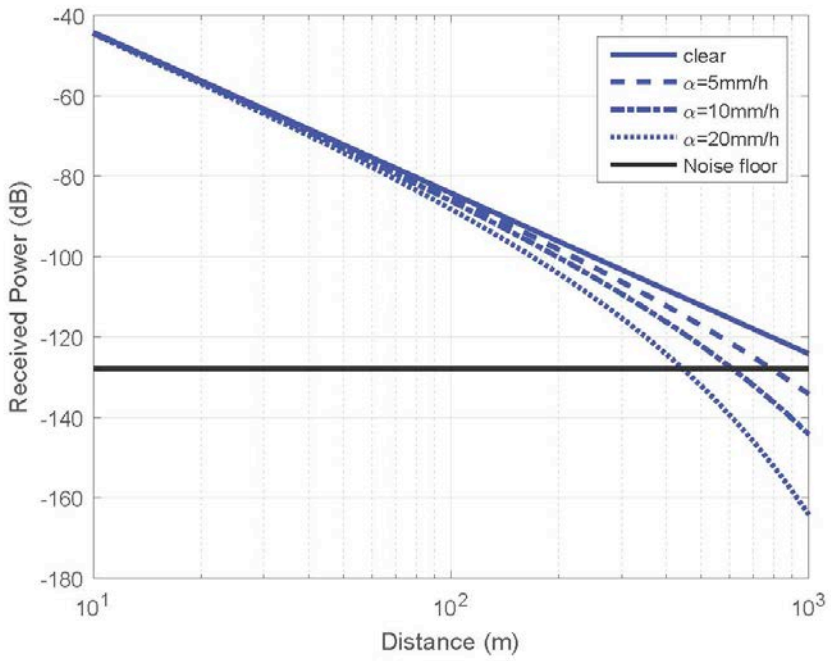

Figure 2.2 FMCW radar signal level under different weather conditions [7]

2.3 Mathematical Model for FMCW Radar System

With the linear frequency modulation, the transmitted signal $s(t)$ can be expressed as

$$s(t) = A\cos\left(2\pi\left(\left(f_c - \frac{BW}{2}\right)t + \frac{BW}{2\Delta t}t^2\right)\right), \tag{2.4}$$

where A is the amplitude of the transmitted signal f_c is the carrier frequency, BW is the transmitted sweep bandwidth and Δt is the sweep time of the transmitted signal.

The received signal from multiple targets, $r_S(t)$, is expressed as

$$r_S(t) = \sum_{i=1}^{M} B_i \cos\left(2\pi\left(\left(f_c - \frac{BW}{2} + f_{d,i}\right)\left(t - t_{d,i}\right) + \frac{BW}{2\Delta t}\left(t - t_{d,i}\right)^2\right)\right), \tag{2.5}$$

where M is the number of targets, B_i is the attenuated amplitude of the i-th received signal, and $t_{d,i}$ and $f_{d,i}$ are delay time and Doppler frequency of i-th received signal, respectively. Note that the noise component is omitted for simplicity in this dissertation.

By the mixer, the transmitted and received signals are multiplied in the time domain and high-frequency components are filtered out by the low-pass filter. The demodulated signal $m_S(t)$, which is made through the mixer and low-

pass filter, is expressed by the following equation

$$m_S(t) = \sum_{i=1}^{M} C_i \cos\left(2\pi\left(\frac{BW}{\Delta t} t_{d,i} - f_{d,i} \right) t + 2\pi\left(f_c - \frac{BW}{2} + f_{d,i} \right) t_{d,i} - \frac{\pi BW}{\Delta t} t_{d,i}^2 \right)$$

, (2.6)

where C_i is the amplitude of the demodulated signal from the i-th target. The demodulated signal is composed of the sum of sinusoidal signals having constant amplitude levels in the time domain. Peaks of the demodulated signals in the frequency domain are observed at certain frequencies having targets' information such as range and velocity. In FMCW radar, such frequency is denoted as the beat frequency $f_{b,i}$ and defined by the following equation,

$$f_{b,i} = \frac{BW}{\Delta t} t_{d,i} - f_{d,i} \quad (2.7)$$

The beat frequency is extracted using a Fourier transform and peak detection algorithm such as a constant false alarm rate (CFAR) method [27]. A spectral component higher than the CFAR threshold is determined as the target peak whose frequency corresponds to the beat frequency. This beat frequency will be used to calculate the range and velocity of targets.

The target SNR is defined as the ratio of the relative magnitude of the target

peak to the noise floor level. It usually shows a value around 30 dB [7] and tends to decrease with distance according to the radar equation. The beat frequency for the distant target usually appears in the high frequency range. Given these facts, one can conclude that the target peaks in the high frequency range shows smaller values than in the low frequency range. The small peaks whose levels are below the lowest quantization level cannot be detected. Therefore, a 20 dB/dec gain on the analog-digital converter (ADC) is applied in practice to increase the detection capability of the small peaks in the high frequency range.

2.4 Signal Processing Structure for FMCW Radar System

In order to extract range and velocity of target, automotive radar detects real target signals in presence of noise and clutters and processes detected signal. In this section, the process for automotive FMCW radar is discussed.

A chirp signal modulated by linear FM is transmitted in the FMCW radar. All signal processing are carried out in up chirp and down chirp region simultaneously. The echo signals which have time delay and frequency offset due to range and velocity of target are received. To extract frequency contained target's information, the transmitted signal and the received signals are multiplied in the mixer. The mixed signal is converted to baseband signal by LPF. By doing these processes, the baseband signal has only frequencies corresponding targets and these frequencies are called beat frequencies. The analog mixed output is converted to digital signal by using Analog-to-Digital Converter (ADC).

By performing Fast Fourier Transform (FFT) algorithm, the mixed signal is converted in frequency domain and the spectrum of signal can be obtained. The beat frequencies are extracted by peak detection algorithm. The ranges and velocities are calculated by using beat frequencies which are extracted in up chirp and down chirp.

All of the above process is expressed in the Figure 2.3.

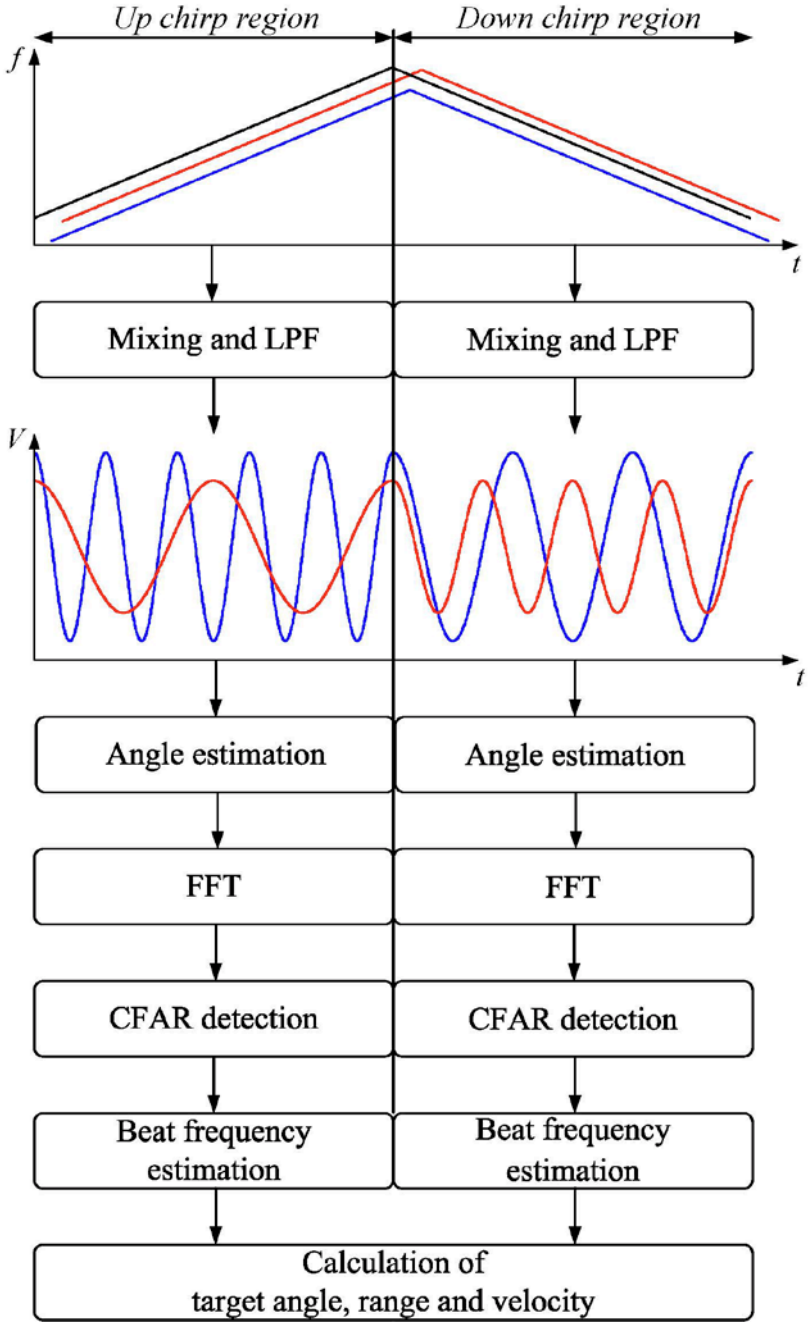

Figure 2.3 Flowchart of signal processing for FMCW Radar system

2.5 Waveform Design for FMCW Radar System

A linear FMCW radar transmits signal whose carrier frequency is linearly changed along the time. Typical FMCW signal for automotive system is composed of two different periodic chirps signal. The part of positive slope is up-chirp and the part of negative slope is down-chirp. The frequency difference of transmitted and received signal has fixed value for linear FMCW radar. By measuring the frequency difference, range and velocity of targets can be estimated. The method of estimation is discussed as follows.

2.5.1 Stationary Target

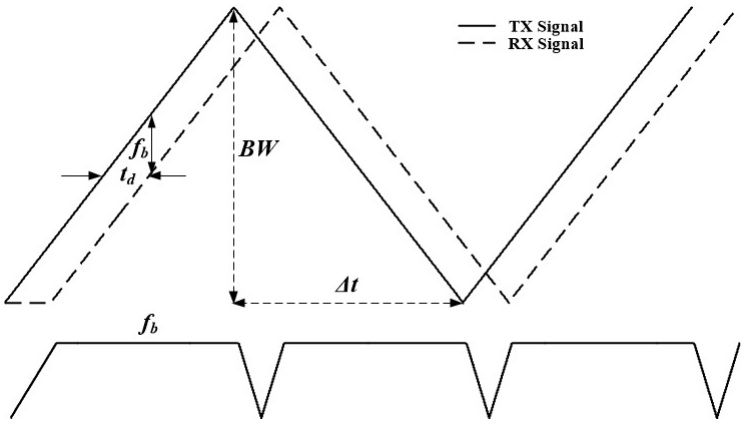

Figure 2.4 FMCW waveform for stationary target and beat frequency

In Figure 2.4, the solid line is transmitted signal and the dashed line is received signal. Beat frequency is depicted in the lower graph in Figure.

When target is a stationary object, the received signal have no offset in the frequency domain as compared to the transmitted signal. Therefore, the beat frequency in the up-chirp and down chirp region are same.

The beat frequency f_b is

$$f_b = \frac{BW}{\Delta t} t_d = \frac{2R \cdot BW}{c\Delta t} = f_r , \tag{2.8}$$

where f_r is the frequency shift due to time delay of target range. Range is computed using (2.8).

$$R = \frac{f_r \cdot c\Delta t}{2BW} . \tag{2.9}$$

2.5.2 Moving Target

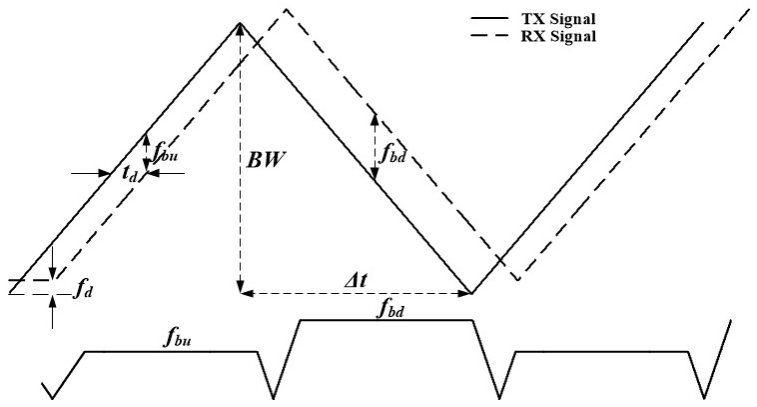

Figure 2.5 FMCW waveform for moving target and beat frequency

In the case of moving target, the received signal contain not only frequency shift due to time delay, but also Doppler frequency. The case which Doppler frequency is considered is depicted in Figure 2.5. The Doppler shift due to relative velocity is

$$f_d = \frac{2V_r}{c} f_c \tag{2.10}$$

where f_c is carrier frequency. Because of Doppler frequency, the beat frequency in up-chirp and down-chirp region is different each other. The beat frequency in up-chirp region f_{bu} follows that

$$f_{bu} = f_r - f_d = \frac{BW \cdot t_d}{\Delta t} - f_d \,. \tag{2.11}$$

Similarly, the beat frequency in down-chirp region f_{bd} is expressed as

$$f_{bd} = f_r + f_d = \frac{BW \cdot t_d}{\Delta t} + f_d \,. \tag{2.12}$$

The frequency shift due to time delay f_r is computed by adding (2.11) and (2.12),

$$f_r = \frac{f_{bu} + f_{bd}}{2} \,. \tag{2.13}$$

Also, the Doppler shift can be computed by subtracting (2.11) from (2.12),

$$f_d = \frac{f_{bd} - f_{bu}}{2}. \tag{2.14}$$

Range is computed by substituting for (2.13) in (2.9),

$$R = \frac{f_r \cdot c\Delta t}{2BW} = \frac{\left(f_{bu} + f_{bd}\right) \cdot c\Delta t}{4BW}. \tag{2.15}$$

The relative velocity is computed by substituting for (2.14) in (2.10),

$$V_r = \frac{\left(f_{bd} - f_{bu}\right) \cdot c}{4 f_c}. \tag{2.16}$$

2.5.3 Resolution

Range resolution can be computed as follow,

$$\Delta R = \frac{c\Delta t}{2BW} \cdot \Delta f = \frac{c\Delta t}{2BW} \cdot \frac{f_s}{N_s} \tag{2.17}$$

where f_s is the sample frequency and N_s is the number of samples. Generally, because that $\Delta f \approx \frac{1}{\Delta t}$, range resolution can be redefined,

$$\Delta R = \frac{c}{2BW}. \tag{2.18}$$

For example, if the sweep bandwidth is 500 MHz, radar system has range resolution of 0.3 m.

Velocity resolution can be computed as follow,

$$\Delta V = \frac{c}{2f_c} \cdot \Delta f = \frac{c}{2f_c} \cdot \frac{f_s}{N_s}. \tag{2.19}$$

2.6 Target Peak Detection for FMCW Radar System

The main task of radar is to detect all objects within the area of observation and to estimate their range and velocity. If all objects were located in front of already known or empty background, the targets will be easily detected. In such a case, the targets can be detected by comparing the fixed threshold computed by pre-analyzing the background. However, in real radar system, the background of target is filled with undesired noise and clutters. Not only the noise and clutter cannot be known statistically, but also target signal is mixed to noise and clutter and cannot be detected by fixed threshold.

For detection to target in real situation, threshold must be set by adapting the noise level. If threshold was set to low value, noise signals are detected as target signals. Such a case is called false alarm. On the other hand, if threshold was set to high value, the probability of detection is low because that target signal level which is located far away or reflected from target with small RCS is lower than threshold. The probability of detection can be raised by using special signal processing method, but the automotive radar has to keep the probability of false alarm low.

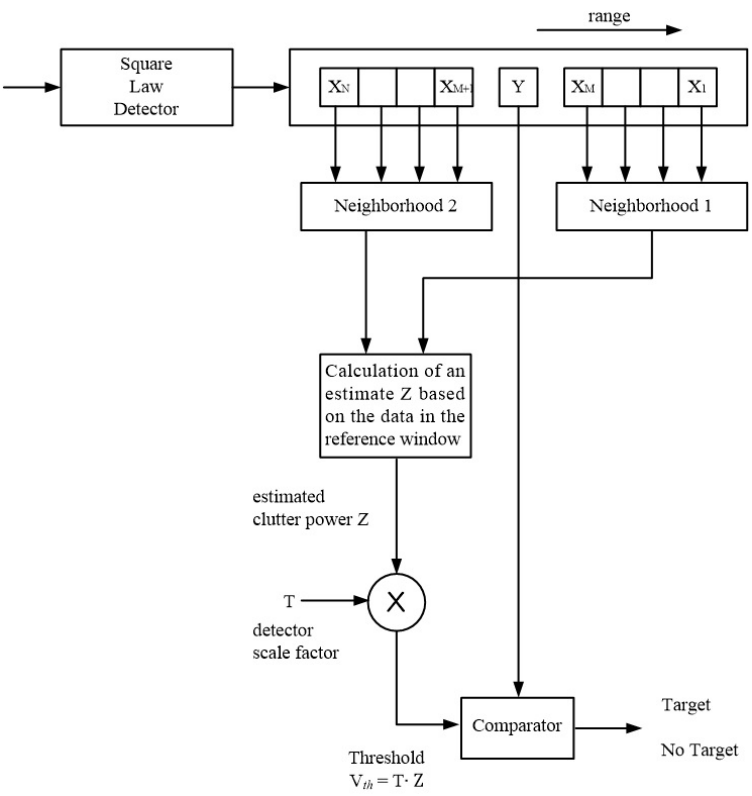

Figure 2.6 General CFAR processor

The false alarm probability is always kept constant in CFAR algorithm by adapting the threshold. The threshold is computed by estimating clutter power of the surrounding environment of the test cell. The procedure of the CFAR algorithm is as follows and is illustrated by Figure 2.6.

1. Measure the mean clutter power level Z.
2. Multiply estimation Z by scaling factor T .
3. $V_{th} = T \cdot Z$ is directly used as the threshold value.

The scaling factor T is a function of method used to estimate μ and also a function of the false alarm probability.

To analyze the detection performance of a CFAR processor in homogeneous background, it is assumed that output of square-law detector in Figure 2.5 follows exponential distribution with probability density function (PDF),

$$f(x) = \frac{1}{\lambda}\exp\left(-\frac{1}{\lambda}\right), \quad x \geq 0 \tag{2.20}$$

where λ is the total background clutter-plus-thermal noise power. Under the null hypothesis H_0 of no target, λ is the background noise power, which is denoted by μ. Under the alternative hypothesis H_1 of presence of a target, λ is $\mu(1+S)$, which S is SNR of the target. Therefore, the value of λ in (2.20) is

$$\lambda = \begin{cases} \mu & \text{under } H_0 \\ \mu(1+S) & \text{under } H_1 \end{cases} \tag{2.21}$$

The CFAR algorithm is divided based on the method used to estimate clutter power. There are many method to estimate clutter power, such as CA, OS [28], CAGO, OSGO, SO, Censored and WCA [29], [30]. Among these method, Cell Averaging (CA) CFAR and Ordered Statistic (OS) CFAR are well known CFAR algorithm.

2.6.1 CA-CFAR

In the CA-CFAR processor, total noise power Z is estimated by arithmetic sum of the reference N cells in the neighborhood of test cell. The CA-CFAR processor is illustrated by figure 2.7 and Z is expressed by (2.22)

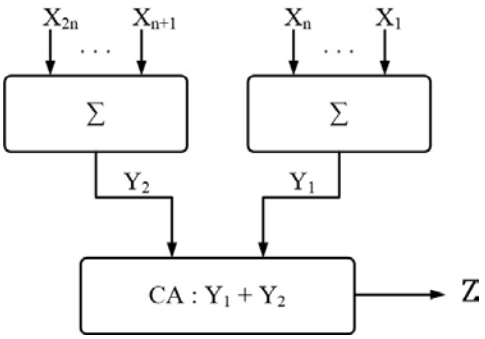

Figure 2.7 CA-CFAR processor

$$Z = \sum_{i=1}^{N} X_i \tag{2.22}$$

where X_i are neighborhood cells surrounding the test cell.

The exponential density is a special case of gamma density with $\alpha = 1$. The PDF of gamma distribution is

$$f(y) = G(\alpha, \beta) = \beta^{-\alpha} y^{\alpha-1} \exp\left(\frac{-y/\beta}{\Gamma(\alpha)}\right), \quad y \geq 0, \alpha \geq 0, \beta \geq 0 . \tag{2.23}$$

where $\Gamma(\alpha)$ is the usual gamma function which has value $(\alpha-1)!$ for integer α. The cumulative distribution function (CDF) of $G(\alpha,\beta)$ cannot be expressed in closed form. However, the characteristic function of $G(\alpha,\beta)$ is

$$\Psi(z)=\frac{1}{(1+\beta)^{\alpha}}. \tag{2.24}$$

Then, X_i follows $G(1,\lambda)$ and Z also follows $G(N,\lambda)$. The false alarm probability can be calculated for a fixed factor T as follows,

$$\begin{aligned} P_{fa} &= E_Z\left\{P\left[Y>TZ \mid H_0\right]\right\} \\ &= (1+T)^{-N} \end{aligned}. \tag{2.25}$$

The constant scale factor T is computed by

$$T=\left(P_{fa}\right)^{1/N}-1. \tag{2.26}$$

It is clear that the false alarm probability is independent of the total noise power μ.

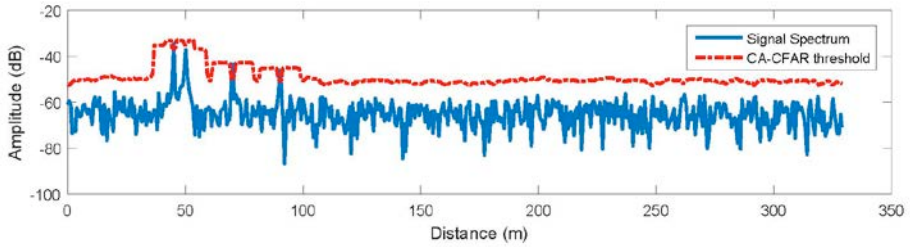

Figure 2.8 CA-CFAR with $P_{fa} = 10^{-6}$ and $N = 24$

The red dotted line in Figure 2.8 is threshold which is obtained by the CA-CFAR processor with $P_{fa} = 10^{-6}$ and $N = 24$. When target peak is in the reference cell, threshold value is high. Because that in the CA-CFAR processor, total noise power is estimated by using reference cells except for test cell, when target peak is in test cell, threshold value is decreased in a moment and target is detected. But, it is confirmed that CA-CFAR algorithm cannot perfectly detect targets which is located closely. Therefore, the CA-CFAR is not efficient for multi target detection.

2.6.2 OS-CFAR

In the OS-CFAR processor, total noise power Z is estimated by k-th largest sample X_k of the reference N cells in the neighborhood of test cell. The OS-CFAR processor is illustrated by figure 2.9.

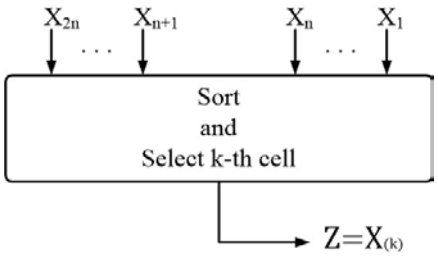

Figure 2.9 OS-CFAR processor

Before analyzing the detection performance of the OS-CFAR processor, consider n independent trials such that on each trial, the result is exactly one of the event $A_1, A_2, \cdots, A_r$ with probabilities $p_1, p_2, \cdots, p_r$ respectively. Then the probability that A_1 occurs exactly n_1 times, $\cdots$, A_r occurs n_r times is

$$\frac{n!}{n_1!n_2!\cdots n_r!} {p_1}^{n_1} {p_2}^{n_2} \cdots {p_r}^{n_r} \tag{2.27}$$

where the p_i are nonnegative real numbers that sum to 1 and n_i are nonnegative integers that sum to n.

Now let $X_1, X_2, \cdots, X_n$ be i.i.d with pdf $f(x)$ and cdf $F(x)$. Let $Y_1 < Y_2 < \cdots < Y_n$ be the X_i's arranged in increasing order, so that Y_k is the k th smallest sample and Y_k's are called the order statistics of the X_i's. The probability that $Y_n \le x$ is the probability that $X_i \le x$ for all i. Using $P\{X_i \le x\}$ is $F(x)$ and X_i is i.i.d., the probability that $Y_n \le x$ is

$$\begin{aligned} F_{Y_n}(x) &= \left[F(x)\right]^n \\ f_{Y_n}(x) &= n\left[F(x)\right]^{n-1} f(x) \end{aligned} . \tag{2.28}$$

Similarly,

$$P\{Y_1 > x\} = \prod_{i=1}^{n} P\{X_i > x\} = \left[1 - F(x)\right]^n . \tag{2.29}$$

Consider that there are $k-1$ random variables less than x, one random variable between x and $x+dx$, and $n-k$ random variables greater than x. Using (2.27), the pdf of ordered statistic $f_{Y_k}(x)$ can be expressed by (2.30),

$$f_{Y_k}(x) = \frac{n!}{(k-1)!1!(n-k!)}\left[F(x)\right]^{k-1}\left[1-F(x)\right]^{n-k} f(x). \tag{2.30}$$

The false alarm probability can be calculated by a fixed T as follows,

$$\begin{aligned} P_{fa} &= E_Z\left\{P\left[Y \geq TX_k \mid H_0\right]\right\} = \int_0^\infty P\left[Y \geq Tx\right] f_{X_k}(x)\,dx \\ &= \prod_{i=0}^{k-1} \frac{(N-i)}{(N-i+T)} \end{aligned} . \tag{2.31}$$

The constant scale factor T given k is computed by solving iteratively for fixed N and P_{fa}. It is also confirmed that the false alarm probability is

independent of the total noise power μ.

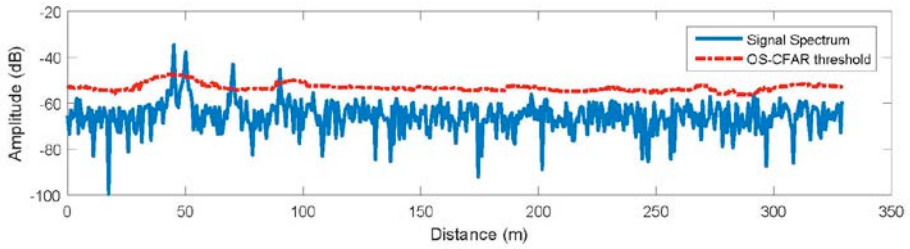

Figure 2.10 OS-CFAR with $P_{fa} = 10^{-6}$ and $N = 24$

Comparing Figure 2.8, OS-CFAR threshold values in Figure 2.10 are stable without severe changes. When target peak is in the reference cell, because that target peak value is the largest, it does not have an effect on k-th largest sample. As the road are crowed with cars, the OS-CFAR is more efficient for multi target detection than the CA-CFAR.

2.7 High-resolution Angle Estimation Algorithm for FMCW Radar System

In order to estimate accurate location of target, not only range and velocity but also angle should be estimated. Particularly, angle estimation is needed in multiple target environment. When two targets are located at same distance with different angles, the beat frequencies of two targets are estimated to same value. From estimating the beat frequency of targets, two targets cannot be distinguished. Hence, two targets located at same distance can be distinguished through angle estimation.

For angle estimation, the signals which received from antenna array are needed. Consider the uniform linear array (ULA) which has M elements with equally spacing d. Then, the phase difference between elements is expressed by

$$\Delta\phi = 2\pi \frac{d}{\lambda} \sin\theta, \tag{2.32}$$

where θ is incoming angle of incident wave. Using the phase difference, angle of target can be estimated.

In array signal processing for angle estimation, there are Bartlett estimation [31], linear prediction, Capon estimation [32] and multiple signal classification (MUSIC) [33] classified as spectral approach. Specially, MUSIC is divided in subspace based method. The maximum likelihood (ML)

[34], [35] and estimation of signal parameter via rotational invariance technique (ESPRIT) [36] are classified as parametric approach. Among these array signal processing, MUSIC and ESPRIT are representative high-resolution estimation. In this dissertation, MUSIC is used as the algorithm for the direction of arrival (DOA) estimation.

The signals received from ULA are expressed as

$$\begin{bmatrix} x_1[n] \\ x_2[n] \\ \vdots \\ x_M[n] \end{bmatrix} = \begin{bmatrix} \mathbf{a}(\theta_1) & \mathbf{a}(\theta_2) & \cdots & \mathbf{a}(\theta_D) \end{bmatrix} \begin{bmatrix} s_1[n] \\ s_2[n] \\ \vdots \\ s_D[n] \end{bmatrix} + \begin{bmatrix} w_1[n] \\ w_2[n] \\ \vdots \\ w_M[n] \end{bmatrix} \tag{2.33}$$

or

$$\mathbf{x}[n] = \mathbf{A}\mathbf{s}[n] + \mathbf{w}[n], \tag{2.34}$$

where

$$\mathbf{a}(\theta_i) = \begin{bmatrix} 1, & e^{j2\pi d/\lambda \sin(\theta_i)}, & \cdots, & e^{j2\pi(M-1)d/\lambda \sin(\theta_i)} \end{bmatrix}^T. \tag{2.35}$$

In (2.33), M is the number of array elements, D is the number of the incident wave, $\mathbf{s}[n]$ is the desired signal, $\mathbf{w}[n]$ is additive noise and $\mathbf{a}(\theta_i)$ is the steering vector. The steering vector is represented as the phase difference due to antenna spacing. It is assumed that noise follows zero mean

complex Gaussian distribution with variance of σ^2, and the desired signal and noise are uncorrelated.

The covariance matrix of the received signals can be obtained as

$$\begin{aligned}\mathbf{R} &= E\left[\mathbf{x}[n]\mathbf{x}^H[n]\right] = \mathbf{A}E\left[\mathbf{s}[n]\mathbf{s}^H[n]\right]\mathbf{A}^H + E\left[\mathbf{w}[n]\mathbf{w}^H[n]\right], \\ &= \mathbf{A}\mathbf{R}_{\mathbf{ss}}\mathbf{A}^H + \sigma^2\mathbf{I}_M\end{aligned} \tag{2.36}$$

where $E[\cdot]$ denotes statistical expectation. In radar system, statistical expectation is replaced with ensemble average,

$$\mathbf{R} \approx \frac{1}{N}\sum_{n=1}^{N}\mathbf{x}[n]\mathbf{x}^H[n]. \tag{2.37}$$

From (2.36), it is confirmed that the covariance matrix can be divided by signal subspace and noise subspace using eigen decomposition. It is expressed as

$$\mathbf{R} = \mathbf{E}_\mathbf{s}\mathbf{\Lambda}_\mathbf{s}\mathbf{E}_\mathbf{s}^H + \mathbf{E}_\mathbf{w}\mathbf{\Lambda}_\mathbf{w}\mathbf{E}_\mathbf{w}^H, \tag{2.38}$$

where $\mathbf{E}_\mathbf{s}$ is $(M \times D)$ the matrix consisting of eigen vectors of signal subspace, $\mathbf{\Lambda}_\mathbf{s}$ is $(D \times D)$ the diagonal matrix consisting of eigen values of signal subspace, $\mathbf{E}_\mathbf{w}$ is $\left(M \times (M-D)\right)$ the matrix consisting of eigen vectors of noise subspace and $\mathbf{\Lambda}_\mathbf{w}$ is $\left((M-D) \times (M-D)\right)$ the diagonal

matrix consisting of eigen values of noise subspace.

Due to orthogonality of $\mathbf{A}$ and $\mathbf{E}_{\mathbf{w}}$, the pseudo spectrum of MUSIC algorithm can be obtained [33] as

$$P_{MUSIC}(\theta) = \frac{\mathbf{a}(\theta)\mathbf{a}^{H}(\theta)}{\mathbf{a}^{H}(\theta)\mathbf{E}_{\mathbf{w}}\mathbf{E}_{\mathbf{w}}^{H}\mathbf{a}(\theta)}. \tag{2.39}$$

By (2.39), when θ is the desired angle, the pseudo spectrum has the largest value due to steering vector and eigen vector of noise subspace as shown in Figure 2.11.

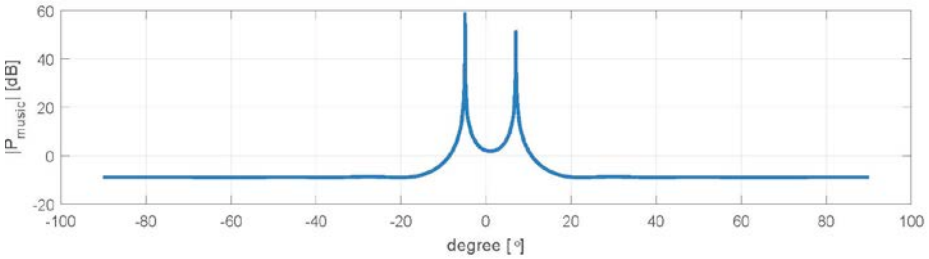

Figure 2.11 The pseudo spectrum of MUSIC when two targets

The performance of MUSIC algorithm is outstanding compared to conventional algorithm. However, because that MUSIC algorithm is based on subspace, there is the possibility of failure to resolve closely spaced signals if the signal subspace and noise subspace are incorrectly separated when the number of samples is small and SNR is low.

Chapter 3. Analysis of Interference in FMCW radar system

3.1 Introduction

In this chapter, the interference between FMCW radars is analyzed. Up to now, the interference has not been researched because that there are not many vehicles equipped radar on road. Therefore the possibility of the interference was low, but it is tend to have gradually increase radar equipped vehicles.

The simple interference scenario is shown in Figure 3.1. There are many reason for the interference.

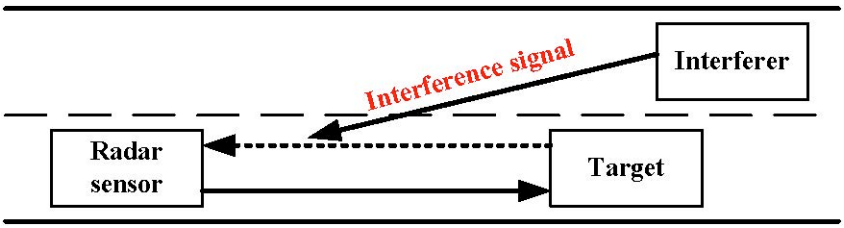

Figure 3.1 The simple interference scenario with one target and one interferer

Due to the sidelobe of antenna beam pattern, the interference can be generated. While the signal level drops, the interference level is higher than returned target signal level. Because that the vehicles recently become rounded shape, the vehicles will scatter incident wave isotopically. Hence, due to effect of

sidelobe and body shape, significant proportion of the reflected signal from the target vehicles within main beam and sidelobe will be scattered to the other antenna. There will be some frequency overlap due to limited operating band of radars, then the interference can be generated as vehicles equipped with radar increase. Also the interference exists due to random sweep phase in identical radar system and different sweep frequency in similar radar system. These effects are particularly analyzed with simulation results in this chapter.

The fundamental radar equation is modified in the section 2. From modified radar equation, the level of interference signal can be predicted. Also, mathematical model is re-modeled by scenarios of interference signal. In the section 4, the interference signal classified by the band of beat frequency and the effect of interference is analyzed with simulation.

3.2 Radar Equation with Interference

When two vehicles equipped radars are along a straight road such that they are each within the main lobe of the other's antenna, then the received signal level can be represented as following steps.

If two vehicles are separated by a distance R, the received density S_I at one vehicle is

$$S_I = \frac{P_t G_t}{4\pi R^2}. \tag{3.1}$$

The effective aperture A_e is

$$A_e = \frac{G_r \lambda^2}{4\pi}. \tag{3.2}$$

The total received power is the product of the effective aperture and the power density

$$P_r = \frac{P_t G_t}{4\pi R^2} A_e = \frac{P_t \lambda^2 G_t G_r}{(4\pi)^2 R^2}. \tag{3.3}$$

Equation can be converted to decibel levels as follows.

$$P_r = P_t + 20\log\left(\frac{\lambda}{4\pi}\right) + G_t + G_r - 20\log(R) - \alpha R_{km}. \tag{3.4}$$

The interference signal level can be predicted by (3.4). The received power from the interferer at various ranges and weather conditions is shown in Figure. Comparing the signal level in Figure 3.2 and Figure 2.2, the received signal level from interferer at 200 m in clear weather is about 60 dB greater than that from RCS of 1 m^2 target in the same conditions.

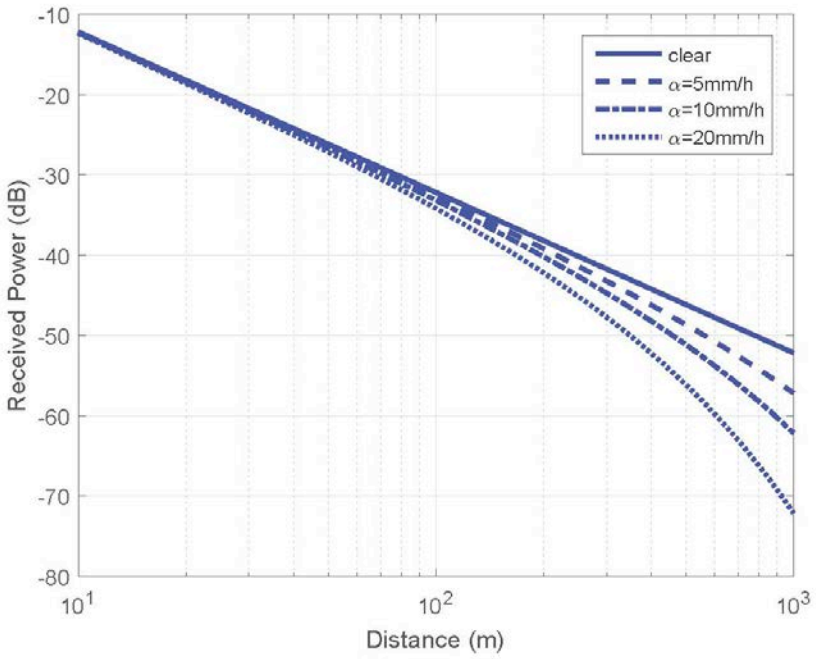

Figure 3.2 Interference levels under different weather conditions [7]

3.3 Mathematical Model with Interference for FMCW Radar System

Interference signals can be classified into two cases depending on its propagation path. One is a direct signal from a vehicle driving in the opposite direction, and the other is an indirect signal which is reflected multiple times by several targets. Both the direct and indirect interference signal levels can be estimated by the radar equation. The amplitude of the direct interference signal is typically in the range of 30-56 dB above the target peak level [7]. Apparently, the direct interference has greater effect on the target peak detection than the indirect interference.

The total received signal $r(t)$ is a summation of the target signal $r_S(t)$ interference signal $r_I(t)$ and the thermal noise $n(t)$. Considering different carrier frequencies ($f_{c,i}^I$), sweep bandwidths (BW_i^I) and sweep times (Δt_i^I), the interference signal can be represented by

$$r_I(t) = \sum_{i=1}^{N} B_i^I \cos\left(2\pi \left(\left(f_{c,i}^I - \frac{BW_i^I}{2} + f_{d,i}^I \right)\left(t - t_{d,i}^I\right) + \frac{BW_i^I}{2\Delta t_i^I}\left(t - t_{d,i}^I\right)^2 \right) \right), \quad (3.5)$$

where N is the number of interferer, and the symbol I denotes the interference signal.

The chirp slope of the interference signal, which is determined by Δt^I and BW^I, may or may not be the same as that of the transmitted signal. If the slopes are in the same value and the time delay of the interference signal is

within the maximum delay time, $t_{d_{max}} = 2R_{max}/c$ the interference is treated as a ghost target and cannot be canceled out with any kinds of effort. As this barely happens in practice, it is out of scope of this dissertation.

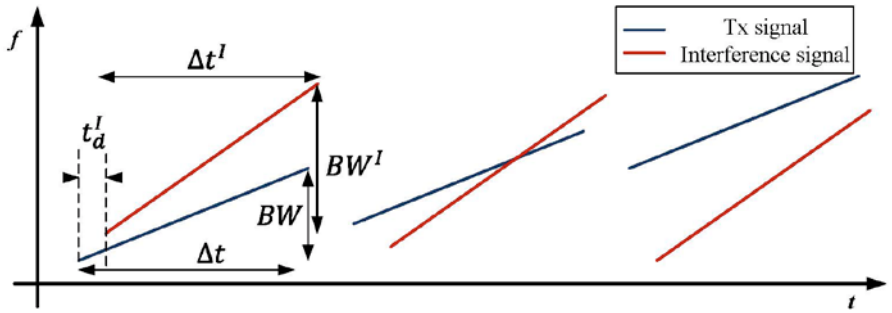

Figure 3.3 The case of mixing signals: Same-Sign Case

The output of FMCW radar system can have two cases according to the mixing conditions. For the first case, both the transmitted and the interference signal have linearly increasing or decreasing instantaneous frequencies (same-sign case, Figure 3.3). The mixer output for the same-sign case is expressed by the following equation,

$$\begin{aligned} m(t) &= m_S(t) + m_I^{SS}(t) \\ &= m_S(t) \\ &\quad + \sum_{i=1}^{N} C_i^I \cos\left\{ 2\pi\left(\left(f_c - f_{c,i}^I \right) \mp \left(\frac{BW}{2} - \frac{BW_i^I}{2} \right) \pm \left(\frac{BW_i^I}{\Delta t_i^I} t_{d,i}^I \pm f_{d,i}^I \right) \right) \right., \\ &\quad \left. \pm \pi\left(\frac{BW}{\Delta t} + \frac{BW_i^I}{\Delta t_i^I} \right) t^2 + 2\pi\left(f_{c,i}^I \mp \frac{BW_i^I}{2} + d_{d,i}^I \right) t_{d,i}^I \mp \frac{\pi BW_i^I}{\Delta t_i^I} t_{d,i}^{I\,2} \right) \end{aligned} \quad (3.6)$$

where $m_I^{SS}(t)$ denotes the mixer output of the interference signal for the same-sign case.

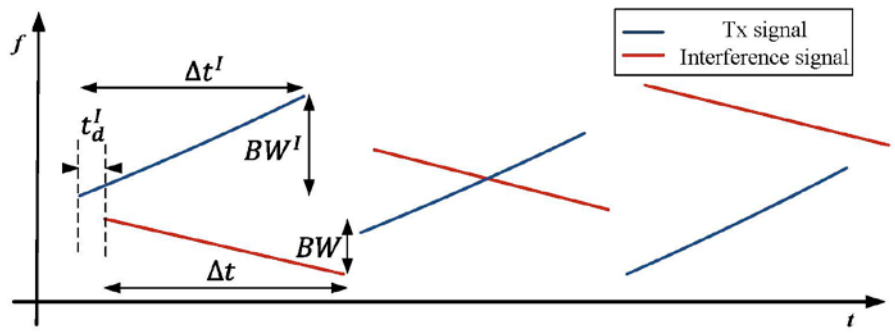

Figure 3.4 The case of mixing signals: Different-Sign Case

For the second case, the transmitted signal has a linearly decreasing instantaneous frequency and the interference signal has a linearly increasing instantaneous frequency or vice versa (different-sign case, Figure 3.4). The mixer output for the different-sign case is given by the following equation,

$$\begin{aligned} m(t) &= m_S(t) + m_I^{DS}(t) \\ &= m_S(t) \\ &\quad + \sum_{i=1}^{N} C_i^I \cos\left(2\pi\left(\left(f_c - f_{c,i}^I \right) \mp \left(\frac{BW}{2} + \frac{BW_i^I}{2} \right) \mp \left(\frac{BW_i^I}{\Delta t_i^I} t_{d,i}^I \pm f_{d,i}^I \right) \right) \right), \\ &\quad \pm \pi\left(\frac{BW}{\Delta t} + \frac{BW_i^I}{\Delta t_i^I} \right) t^2 + 2\pi\left(f_{c,i}^I \pm \frac{BW_i^I}{2} + d_{d,i}^I \right) t_{d,i}^I \pm \frac{\pi BW_i^I}{\Delta t_i^I} t_{d,i}^{I\,2} \end{aligned} \qquad (3.7)$$

where $m_I^{DS}(t)$ denotes the mixer output of the interference signal for the different-sign case.

The rest of this dissertation deals with the mixer output signal in the digital domain. We denote the k-th time sample of the $m(t)$ as m_k, and the collection of m_k s within an observation snapshot as $\mathbf{m} = [m_0, m_1, \cdots, m_{K-1}]^T$. K is the number of the time samples in a snapshot.

3.4 Type of Interference between FMCW Radars

The mutual interference in FMCW radar systems can be divided into two types, wide band and narrow band, depending on the portion of the interference beat frequency occupying the low pass filter (LPF) passband. For simplicity, regarding the beat frequency of the interference signal, it is assumed that there is one received signal reflected by the target and one interference signal from another FMCW radar system.

3.4.1 Beat Frequency in Narrow Band

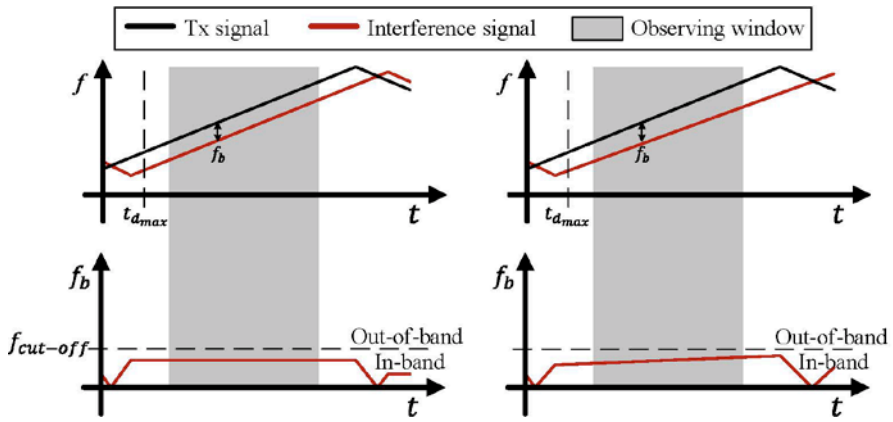

Figure 3.5 Beat frequency in narrow band

An Interference signal comes with a random time delay t_d^I, as it is transmitted from the other radar system. Narrow band interference occurs when the interference accidentally comes with a small time delay such that the

chirp of the interference is in-phase with the chirp of the observer's radar system. Specifically this happens when the t_d^I is within $t_{d_{max}}$, then the interference signal is recognized as target signal. Besides, if the chirp slope of the interference signal is slightly different to the observer's transmitted signal, the bandwidth of beat frequency in this case is small and lies in band.

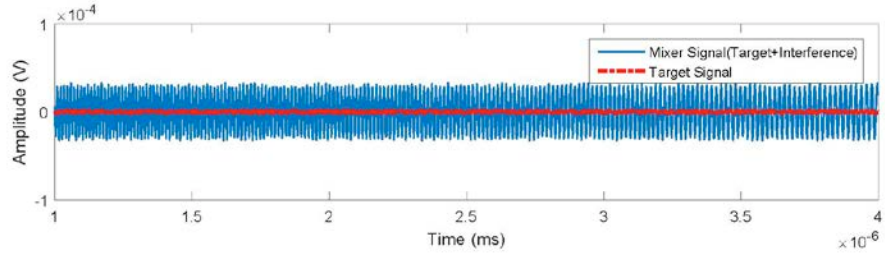

Figure 3.6 Mixer signal when narrow band interference (right case in Figure 3.5)

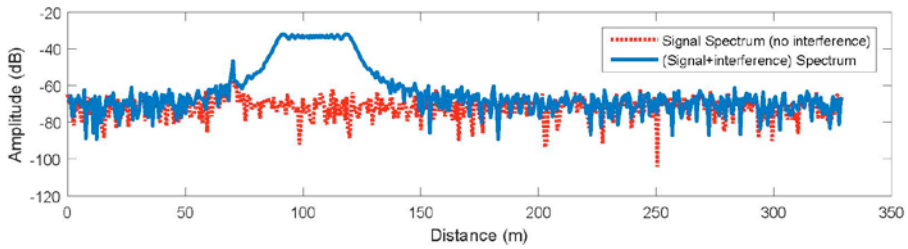

Figure 3.7 Signal spectrum when narrow band interference (right case in Figure 3.5)

As shown in right side Figure 3.5, the beat frequency for the narrow band interference occupies only a small portion of the in-band region in the observing window. Mixer signal contained interference is shown in Figure 3.6.

Because that the power of interference signal is higher than that of target signal, target signal is hidden in the mixer signal. Apparently, there is not specifically changed. However, in the frequency domain, the noise floor is increased through the band corresponding to the small portion as shown in Figure 3.7. Depending on the situation, the target peak can be hidden in the noise floor resulted from narrow band interference and cannot be detected.

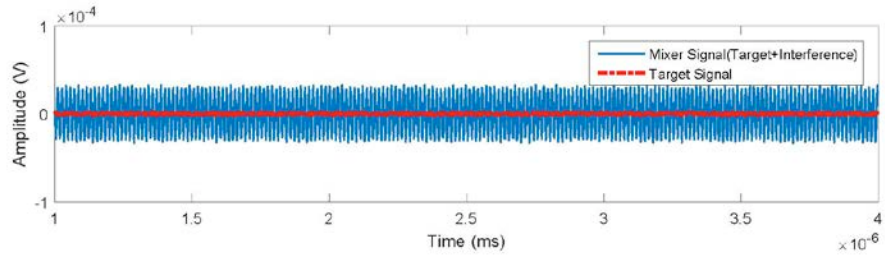

Figure 3.8 Mixer signal when narrow band interference (left case in Figure 3.5)

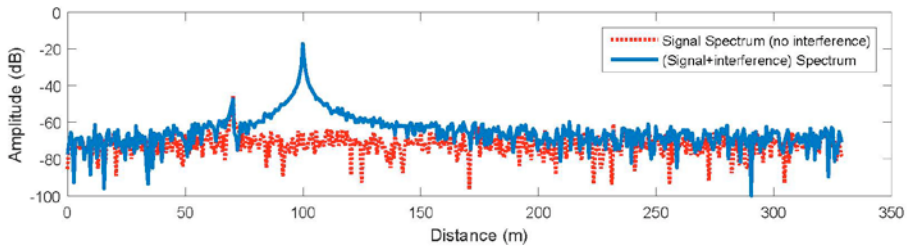

Figure 3.9 Signal spectrum when narrow band interference (left case in Figure 3.5)

If two radar systems are identical, the beat frequency of the interference signal has a single value that does not vary with time as shown left side in

Figure 3.5, since the chirp slopes are the same. In Figure 3.8, mixer signal which contains interference is shown like Figure 3.6. In the frequency domain, the interference looks like a target and it is interpreted as a ghost target at a fixed range as shown in Figure 3.9. Rather, due to high power of interference, the interference peak is larger than target peak. The probability of generating narrow band interference is to be less than 0.0001 [7], so the effect is almost insignificant in general.

3.4.2 Beat Frequency in Wide(entire) Band

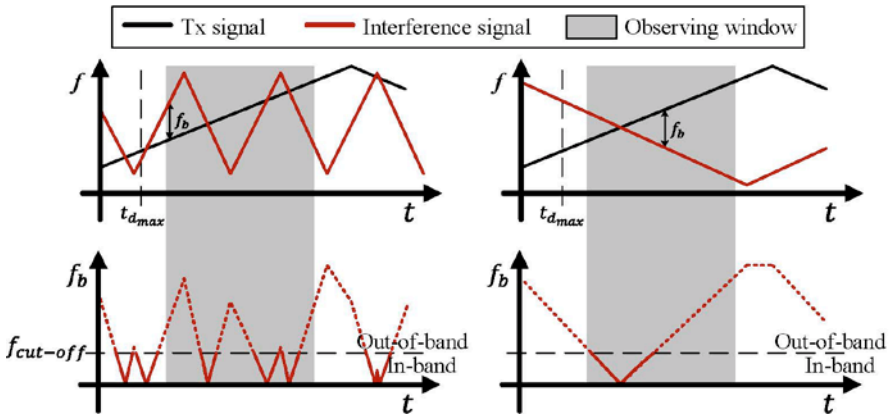

Figure 3.10 Beat frequency in wide band

Two typical scenarios for the wide-band interference occurrence are shown in Figure 3.10. The plots in the right side are for when t_d^I is beyond t_d^I and the left ones are for when the sweep period of the radar system is significantly different from the observer's. In both cases, the beat frequency lies over both

in-band and out-of-band region. The beat frequency above the cut-frequency, which is plotted as dotted horizontal black line, is filtered out by LPF. Therefore the remaining interference occupies the time portion corresponding to the solid red line in the bottom of Figure 3.10. For this sparse occurrence in the time domain, the wide-band interference is also referred to as transient interference in the literature.

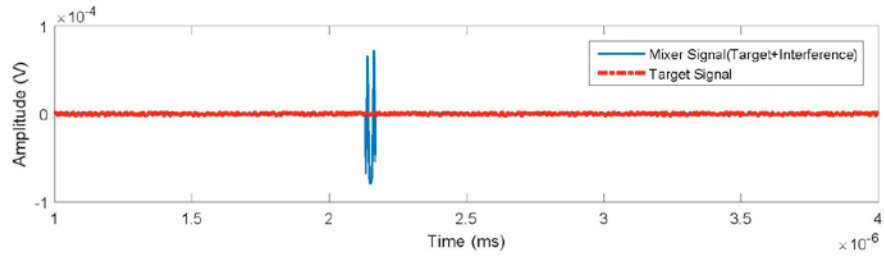

Figure 3.11 Mixer signal when wide band interference (right case in Figure 3.10)

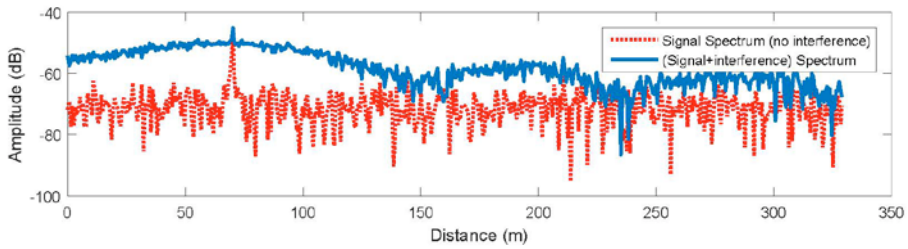

Figure 3.12 Signal spectrum when wide interference (right case in Figure 3.10)

In the case of wide band interference, narrow pulse signal is shown in the time domain as shown in Figure 3.11. Due to high power of interference,

magnitude of pulse signal is larger than that of target signal. In the frequency domain, the wide band interference has the same effect as a white noise. Since the beat frequency has almost constant power in all frequency bins, it causes an increase in the noise floor with some dips throughout the entire frequency domain as shown in Figure 3.12.

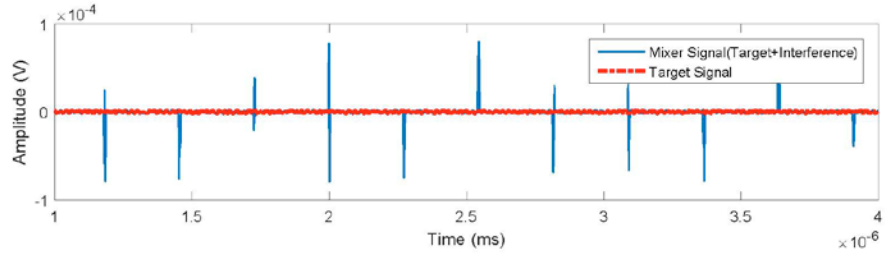

Figure 3.13 Mixer signal when wide band interference (left case in Figure 3.10)

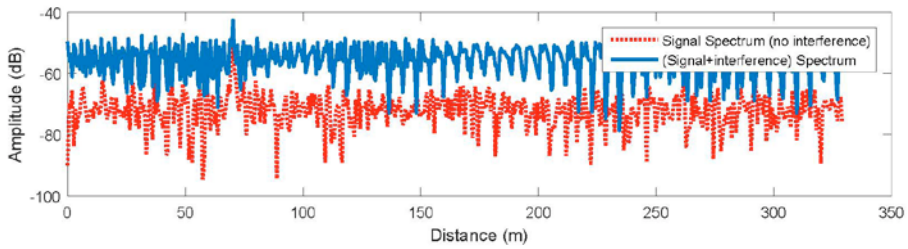

Figure 3.14 Signal spectrum when wide band interference (left case in Figure 3.10)

In the left case in Figure 3.10, many narrow pulse signals appear in the time domain as shown in Figure 3.13. Then, like Figure 3.12, noise floor level is increased in the frequency domain, but many dips are shown in Figure 3.14.

The target SNR is about 30dB in the case of no interference, whereas it is reduced to only 10dB when wide band interference. In particular, given the influence of a strong interference, the noise floor level happens to be above the target peak level and target peak is hidden in the noise floor. The case of wide band interference occurs more frequently than narrow band interference in FMCW radar systems [7]

Chapter 4. The Method for Removing Effects of Interference in FMCW Radar System

4.1 Introduction

In the section 2 of this Chapter, the FMCW interference suppression algorithm is proposed. While its performance is discussed, we make up for the drawback of proposed algorithm. By measurement data, the validity of suppression algorithm is shown. In the section 3, the restoration method for missing region due to the interference is proposed. The missing region is predicted by using linear prediction. For that reason, it is examined whether to apply linear prediction. Its performance also is discussed by simulation results.

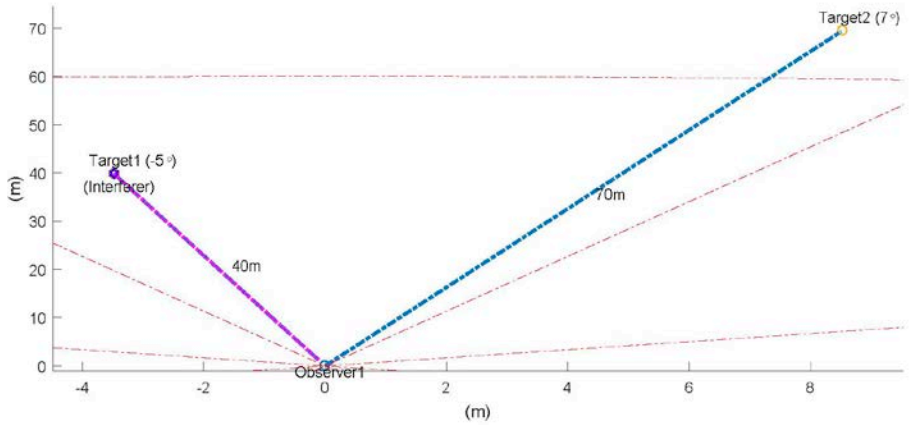

Figure 4.1 Simulation scenario

The simulation is performed by generating the mixer output in the form of a baseband signal based on the system model in the section 2 of Chapter 2 and section 3 of Chapter 3, to avoid the difficulty of generating RF signals at 77 GHz-bands. To examine the performance of the proposed method, simulations were performed under the following conditions as shown in Figure 4.1. Two targets are located 40 m with angle of -5° and 70 m with angle of 7° away respectively from the observer and the target located at 40 m away acts as an interferer as well.

Both the interferer and the observer are equipped with the same FMCW radar systems, of which, a sweep bandwidth and a sweep time are set to 500 MHz and 5 ms, respectively. Also by setting a maximum detection range to 200 m, the maximum delay time $t_{d_{max}}$ becomes 1.33 μs. Assuming that the time delay t_d^I of the interference is 4 ms as shown right side in Figure 3.9, the interference signal behaves as a wide-band interference (case1).

Beat frequency peaks of the frequency response were detected by the ordered-static (OS) CFAR algorithm [28], where the probability of the false alarm is set to 10^{-6} and reference window size is 32.

4.2 Interference Suppression Method

4.2.1 Clipping Algorithm

Clipping is a simple way to reduce the effect of unwanted impulse-like signal on target signal. A typical clipping method considers any signal components outside the threshold value as an unwanted signal, and clips it out.

We propose a clipping algorithm to suppress the interference signal from the mixer output in FMCW radar systems. The algorithm works in two steps.

Clipping Algorithm

1. **Set the upper and lower bound as upper $\alpha\%$ and lower $\alpha\%$ of the mixer output $\mathbf{m}$ defined in section 2, respectively.**

2. **Clip out the mixer output above the upper bound and below the lower bound.**

The algorithm sets the threshold by tuning the value of α in step 1, which is used to find the interference signal portion in the time domain. When α is set too large, the algorithm clips out even the target signal as well as the interference signal, and the target information will be lost. In contrast, when α is set too small the interference signal will not be sufficiently removed. Therefore, it is important to find an optimized value for α to sufficiently suppress the interference while keeping the target information.

However it is very challenging to set α to a proper value. First of all, both the target and interference signal levels are unknown to the radar system. In addition, even if the receiver somehow found a proper value for α for an observation snapshot, this cannot be used again in the next snapshot, as the SIR varies in time.

4.2.2 WEN Algorithm

This algorithm is suggested in order to compensate drawbacks of the clipping method. The proposed weighted-envelope normalization (WEN) algorithm consists of four steps, as outlined below.

WEN Algorithm

---

1. **Find the forward-sliding window maxima $\mathbf{m}^{F,max}$ of the mixer output $\mathbf{m}$ by calculating**

$$\mathbf{m}^{F,max} = [m_0^{F,max}, m_1^{F,max}, \cdots, m_{K-1}^{F,max}]^T$$

$$m_k^{F,max} = \max_l \left(abs\left(m_{l \bmod K} \right) \right), \quad l = k-L+1, \cdots, k-1, k\,.$$

where L is the size of the sliding window and K is the number of the time samples in a snapshot.

2. **Find the backward-sliding window maxima $\mathbf{m}^{B,max}$ of the mixer**

---

output m by calculating

$$\mathbf{m}^{B,max} = [m_0^{B,max}, m_1^{B,max}, \cdots, m_{K-1}^{B,max}]^T$$

$$m_k^{B,max} = \max_l \left(abs\left(m_{l \bmod K} \right) \right), \quad l = k - L + 1, \cdots, k - 1, k .$$

3. Find the envelope r of the mixer output m by calculating

$$\mathbf{r} = [r_0, r_1, \cdots, r_{K-1}]^T$$

$$r_k = \min_l (m_l^{F,max}, m_l^{B,max}) .$$

4. Normalize the mixer output m with the weighted gain $\mathbf{w} = [w_0, w_1, \cdots, w_{K-1}]$**, where** $w_k = \frac{1}{r_k}$**.**

$$\widetilde{\mathbf{m}} = [w_0 m_0, w_1 m_1, \cdots, w_{K-1} m_{K-1}] .$$

It is noteworthy that the algorithm obtains the sliding window maxima over two steps, one for forward-sliding and the other for backward-sliding. Assuming that only one of the forward- or backward-sliding is applied to find the envelope of the mixer output, some parts of the target signal might be misjudged as the interference signal, as denoted by the dotted circles in Figure

4.2 and Figure 4.3. In step 3, for more accurate detection of the interference signal, the envelope should be obtained by selecting the smaller value of the forward- and backward-sliding window maxima. In Figure 4.4, the envelope obtained in step 3 detects the interference portion accurately. The weighted signal in step 4 is obtained by multiplying the inverse of the envelope value and the mixer output. The interference signal and the magnitude of the envelope generally has a much larger amplitude value than the target signal. Therefore, the weighting process suppresses the signal corresponding to the interference with almost no loss of the target information, as shown in Figure 4.5. Figure 4.6 shows the resultant signal spectrum in the frequency domain. Without the WEN algorithm, the smaller peak cannot be detected by the CFAR algorithm because the target SNR is only about 10 dB (dotted red line). On the other hand, the target SNR becomes greater than 20 dB after applying the proposed WEN algorithm (solid blue line), which guarantees reliable detections for CFAR algorithm.

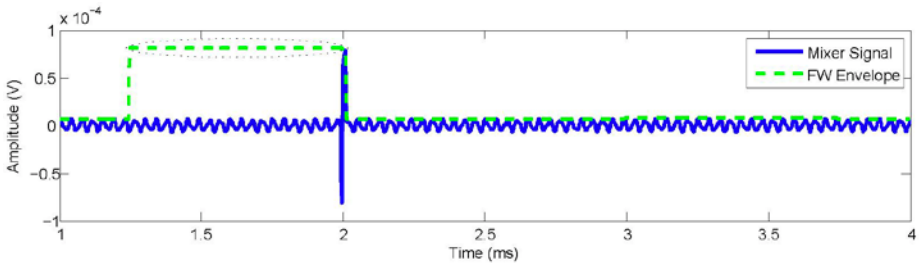

Figure 4.2 Forward-sliding window for WEN (case1)

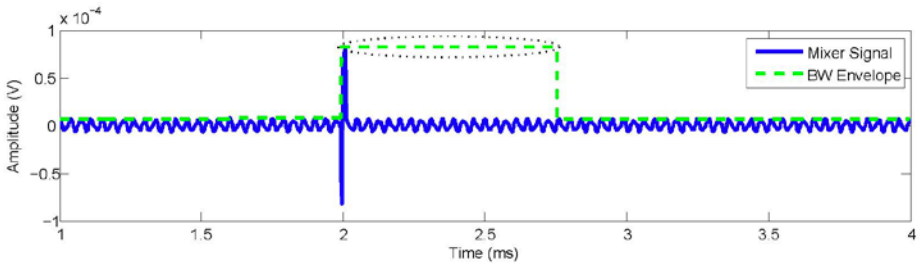

Figure 4.3 Backward-sliding window for WEN (case1)

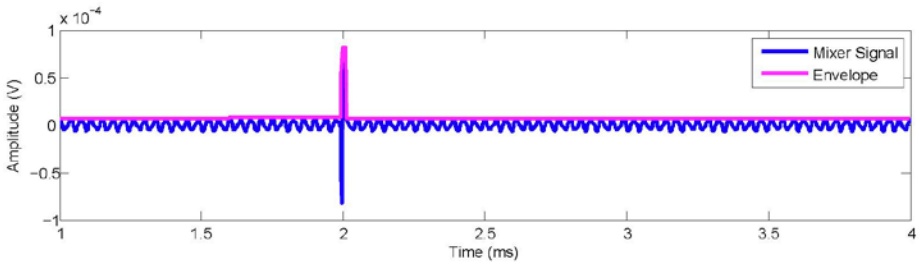

Figure 4.4 Envelope of the mixer signal for WEN (case1)

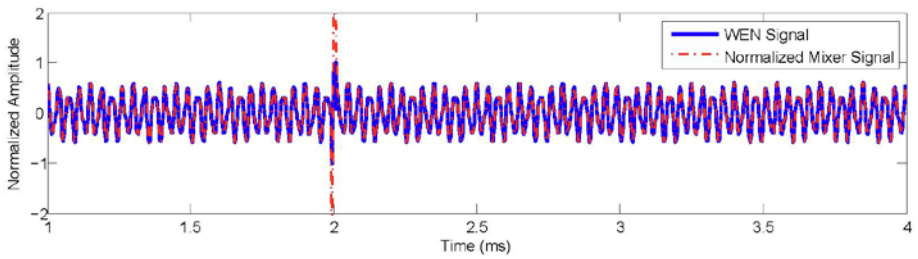

Figure 4.5 WEN signal (case1)

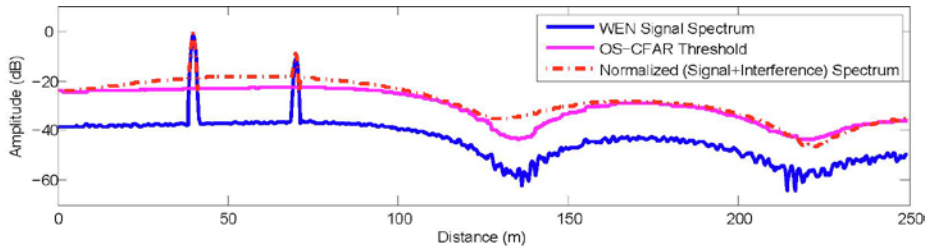

Figure 4.6 Spectrum of WEN signal (case1)

Unfortunately, there are situation where the WEN algorithm cannot be properly applied. Suppose a sweep time and a sweep bandwidth of the interferer's radar system are 0.5 ms and 200 MHz, respectively (case2). Then, two or more interference signals come within a sliding window as in Figure 4.7. In this case, it is impossible to separate the individual interference pulses from each other with WEN algorithm. The envelope for the target signal between the unseparated interference signals is unintentionally set to a large value. Consequently, even the target signal is suppressed as shown in Figure 4.8. The resultant signal spectrum in the frequency domain is depicted in Figure 4.9. The target SNR is not guaranteed sufficiently with the WEN algorithm, so that the peak detection in the frequency domain is difficult to be achieved.

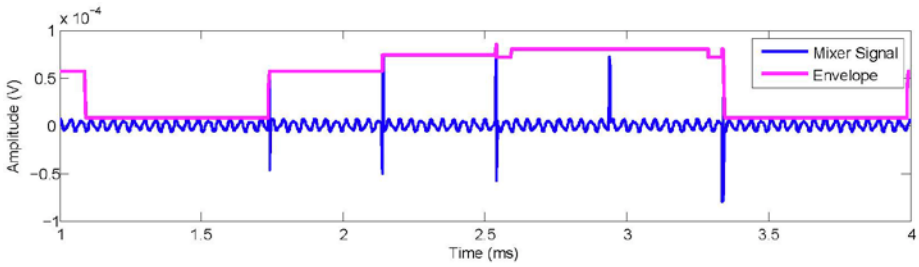

Figure 4.7 Envelope of the mixer signal for WEN (case2)

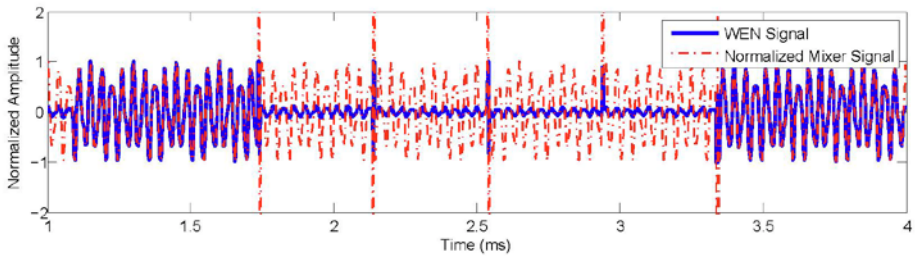

Figure 4.8 WEN signal (case2)

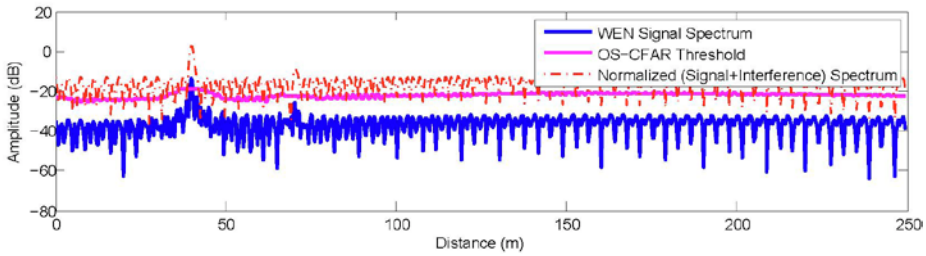

Figure 4.9 Spectrum of WEN signal (case2)

In order to separate the interference signals coming within a short interval, one may use a smaller sliding window for the WEN algorithm. However the sliding window size cannot be infinitely small because it is related to the minimum detectable range of the target. The relation between the minimum

detectable range d_{min} and the minimum sliding window size L_{min} is

$$f_{r,min} = \frac{BW}{\Delta t}\frac{2d_{min}}{c}, \tag{4.1}$$

$$L_{min} = \frac{f_s}{f_{r,min}}, \tag{4.2}$$

where f_s is the sampling frequency of the radar system. As a result, rather than decreasing the sliding window size, some other solution would be needed in order to separate the interference signals coming within a sliding window.

4.2.3 AWEN Algorithm

In this section, a new algorithm is proposed that complements drawbacks of the above two methods. This algorithm provides a reasonable threshold value for clipping out the interference signal and it also separates the pulsed interference signals coming with short intervals.

The proposed algorithm is summarized as follows.

AWEN Algorithm

1. **Find the forward-sliding window maxima $\mathbf{m}^{F,max}$ of the mixer output $\mathbf{m}$ by calculating**

$$\mathbf{m}^{F,max} = [m_0^{F,max}, m_1^{F,max}, \cdots, m_{K-1}^{F,max}]^T$$

$$m_k^{F,max} = \max_l \left(abs\left(m_{l \bmod K} \right) \right), \quad l = k - L + 1, \cdots, k-1, k .$$

where L is the size of the sliding window and K is the number of the time samples in a snapshot.

2. **Find the backward-sliding window maxima $\mathbf{m}^{B,max}$ of the mixer output $\mathbf{m}$ by calculating**

$$\mathbf{m}^{B,max} = [m_0^{B,max}, m_1^{B,max}, \cdots, m_{K-1}^{B,max}]^T$$

$$m_k^{B,max} = \max_l \left(abs\left(m_{l \bmod K} \right) \right), \quad l = k - L + 1, \cdots, k-1, k .$$

3. **Find the envelope $\mathbf{r}$ of the mixer output $\mathbf{m}$ by calculating**

$$\mathbf{r} = [r_0, r_1, \cdots, r_{K-1}]^T$$

$$r_k = \min_l (m_l^{F,max}, m_l^{B,max}) .$$

4. **Normalize the mixer output $\mathbf{m}$ with the weighted gain $\mathbf{w} = [w_0, w_1, \cdots, w_{K-1}]$.**

$$\widetilde{\mathbf{m}} = [w_0 m_0, w_1 m_1, \cdots, w_{K-1} m_{K-1}],$$

where

$$w_k = \begin{cases} \dfrac{1}{T_c} & \text{if } m_k < T_c \\ \dfrac{1}{r_k} & \text{if } m_k > T_c \end{cases} \quad \textbf{and} \quad T_c = (1+\beta)\min_k(r_k), \quad 0 < \beta < 1.$$

We name the proposed algorithm as advanced weighted-envelope normalization (AWEN) algorithm. In the AWEN algorithm, the envelope of the mixer output is obtained by the same procedure as in the WEN algorithm. In step 4, the AWEN adopts a threshold T_c based on the envelope value. The threshold is used to determine whether the mixer output m_k belongs to the interference portion or not. Mixer output m_k is determined to be the target signal if $m_k < T_c$, and is normalized by the reciprocal of the threshold value, $1/T_c$. When $m_k > T_c$, m_k is treated as an interference signal and is normalized by its reciprocal of the envelope value, $1/r_k$.

T_c is calculated with respect to the minimum value of the signal envelope, where β is a control parameter to be designed. As the majority of the interference signal has much larger instantaneous power than the target signal component, it can be said that the threshold value is obtained with respect to the target signal level. This provides more reasonable threshold than the clipping method, in which the threshold is obtained with respect to the largest signal level.

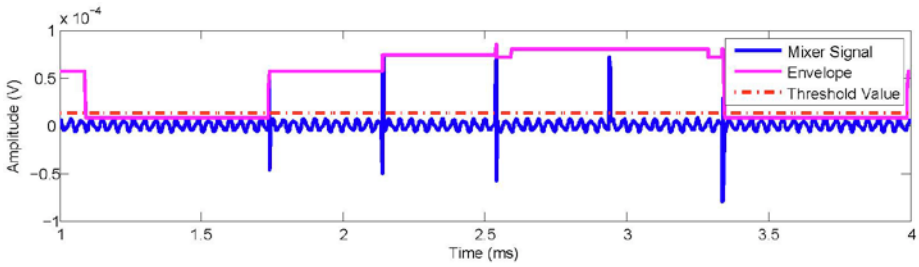

Figure 4.10 Envelope of the mixer signal for AWEN (case2)

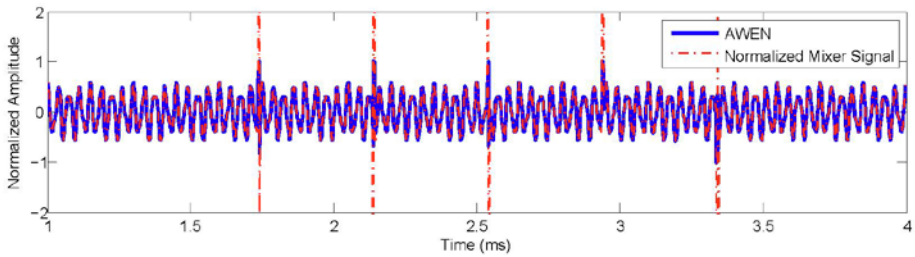

Figure 4.11 AWEN signal (case2)

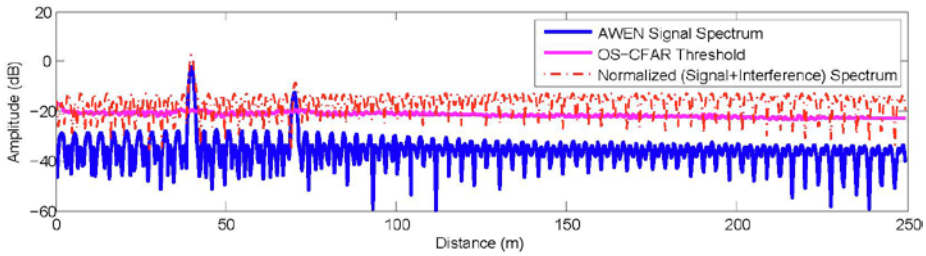

Figure 4.12 Spectrum of AWEN signal (case2)

Figure 4.10 - 12 show the signal processing procedure and the resultant signal of the AWEN algorithm. In Figure 4.10, the signal envelope fails to separate the individual interference pulses, as in WEN algorithm. On the other hand, threshold, depicted by dotted red line, obviously splits the target and

interference signals well. In Figure 4.11, it is confirmed that the interference signal pulses are significantly suppressed. The resultant signal in the frequency domain is plotted in Figure 4.12. Compared to the mixer output signal with no interference suppression (dotted red line), the noise floor is significantly lowered for the AWEN algorithm (solid blue line), while the target peak remained in the same level. Consequently, the sufficient target SNR is achieved for the peak detection using CFAR algorithm. From repetitive performances, target SNR for AWEN is increased on average by 54 times (17 dB) as compared to target SNR for FFT.

As the AWEN algorithm sets the threshold value according only to the target signal level, its performance is irrespective to the magnitude of the interference signal level. If the target SNR for peak detection is guaranteed for the interference-free environment, target peaks are well detected using the AWEN algorithm even in the multiple interferences environment.

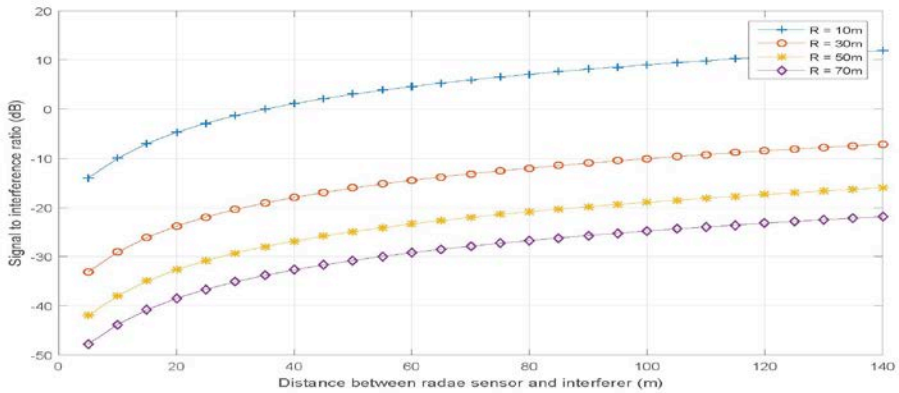

Figure 4.13 The distribution of SIR

The distribution of SIR according to distance between radar sensor and interferer is depicted in Figure 4.13. When target is located at 70 m, the value of SIR drops to -50 dB.

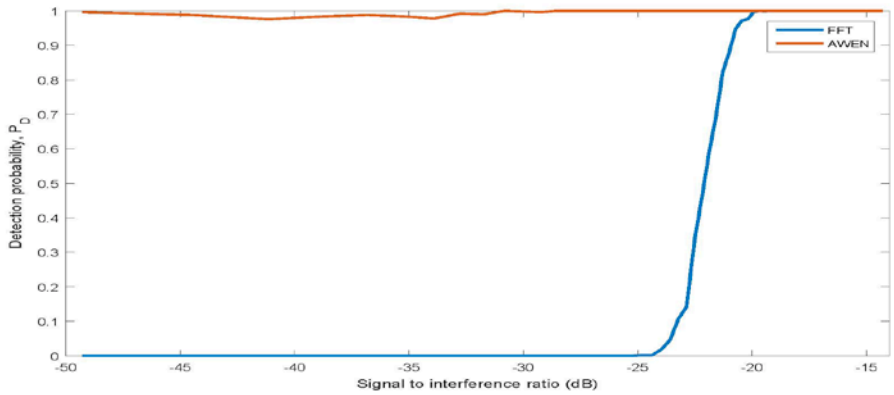

Figure 4.14 The detection probability of FFT and AWEN

In Figure 4.14, the detection probability is represented when target is located at 70 m. The detection probability for conventional FFT starts sharply to drop while the SIR is beyond -20 dB and is zero when the SIR is under -25 dB. From the results of applying AWEN algorithm, it is showed that target can be almost perfectly detected in all region of SIR. Thus, it can be seen that the interference signal is perfectly detected and suppressed regardless of the intensity of the interference.

If much target information are lost in the process of suppressing the interference signals, the sufficient target SNR is not guaranteed as shown in Figure 4.9. Simulations were repeatedly carried out by varying the

interference signal length in one snapshot. From the result, when the sample of the interference signal is more than 35 % in one snapshot, multiple target detection does not work well. But, this case is rare and even if this case ever happens, the target information can be obtained from another snapshot.

4.2.4 Measurement Result

In this section, performance of the proposed AWEN algorithm is verified by measurement using actual automotive FMCW radar systems at an anechoic chamber. For verifying AWEN algorithm, conventional radar is used for observer's radar system and DELPHI radar is used for interferer's radar system. The system parameters of conventional radar are same as those in the section 1 of this chapter. The specification of DELPHI radar is not known exactly, but it is known that DELPHI radar has small sweep time. Hence, the measurement scenario is similar to the left case in Figure 3.9 and this scenario is suitable for verifying AWEN algorithm. There are observer's antenna, interferer's antenna and target simulator which makes a single target virtually. Interferer's antenna and target simulator is located about 5m in front of observer's antenna and target simulator makes a virtual target located about 145 m.

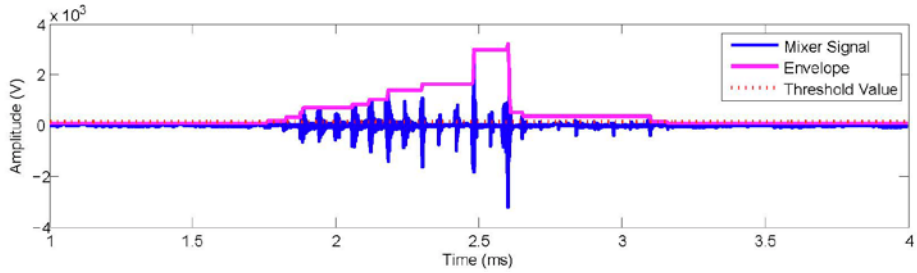

Figure 4.15 Envelope of the mixer signal for AWEN (measurement)

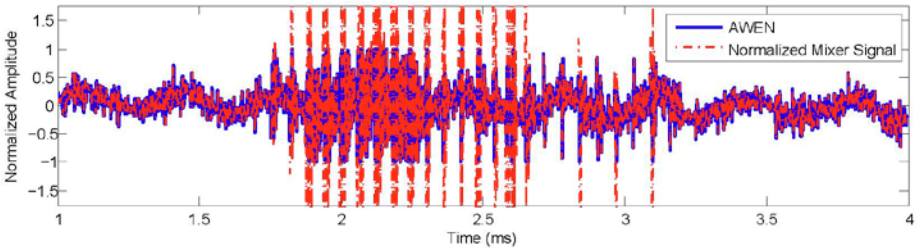

Figure 4.16 AWEN signal (measurement)

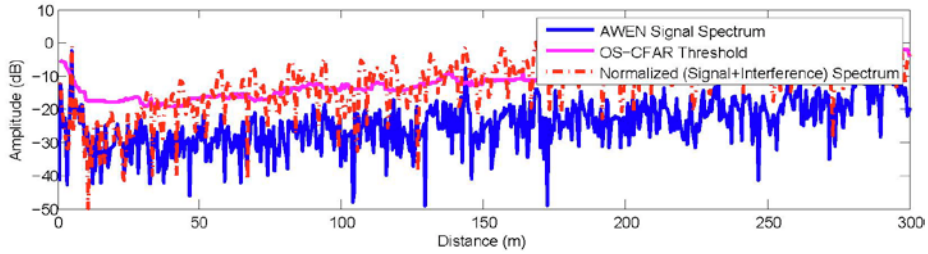

Figure 4.17 Spectrum of AWEN signal (measurement)

The measurement results are shown in Figure 4.15 - 17. In Figure 4.13, the mixer signal between conventional radar and DELPHI radar is depicted. As expected earlier, the interference signals occur multiple times in the one observing window. In this case, AWEN algorithm also works well as shown in

Figure 4.16. It is confirmed that all interference signals are suppressed by a preset threshold value. The red dotted line in Figure 4.17 is the signal spectrum of mixer output before applying the proposed AWEN algorithm. Because of the interference signal, the noise level is increased throughout the entire frequency band. The target SNR corresponding to the target located at 145 m is very low such that the target cannot be detected through CFAR algorithm. As blue line shown in Figure 4.17, the target SNR of 145 m is increased to be approximately 10 dB by AWEN algorithm. As the target SNR is sufficiently increased, target peak is detected by using CFAR algorithm. In conclusion, measurement results also show that the multiple interferences can be suppressed effectively with the proposed AWEN algorithm, as in the simulation results in the previous subsection (4.2.3).

The frame rate of typical FMCW automotive radar is 100 ms [7]. Recently, radar manufacturers require a frame rate of up to 50 ms. The average execution time to obtain the result in Figure 4.15 ~ 17 is about 38 ms. The simulation was carried out using MATLAB. The version of MATLAB is R2014a (8.3.0.532) and the used CPU is Intel(R) Core(TM) i5-4670@3.40GHz. The execution time contains AWEN algorithm, FFT and peak detection algorithm. The processing time with DSP or ASIC can be reduced further to satisfy the requirement of the automotive radar system. Therefore, the execution time of 38 ms is reasonable enough. Because the number of data to be processed is about two thousand samples, the complexity of AWEN is also low and real-time implementation may be possible. In conclusion, measurement results show that AWEN algorithm can effectively

suppress mutual interference as shown in the previous subsection (4.2.3) and the proposed algorithm is sufficiently practical.

4.3 Signal Restoration Method

In the previous section (4.2), it is confirmed that canceling the interference signal in the time domain can lower the noise level in the frequency domain and improve the target detection accuracy significantly. But, the distortion regions still remain in the place that was the interference. Due to this distortion, it is difficult to estimate angles of targets. The pseudo spectrum of MUSIC using AWEN signal for scenario (Figure 4.1) is shown in Figure 4.18. As mentioned in the section 1 of this chapter, desired angles are -5° and 7° (dotted line).

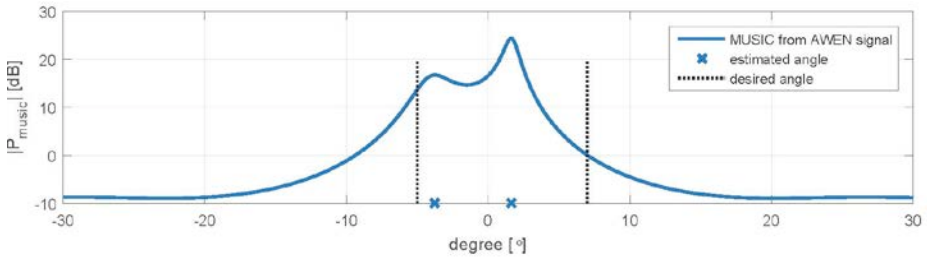

Figure 4.18 Pseudo spectrum of MUSIC for AWEN signal (case2)

For restore the distortion region which is still remained after suppressing the interference, the missing region is predicted by linear prediction using AR model. To more precisely predict the signal, the window function is proposed.

4.3.1 Linear Prediction

Consider that a signal s_n is the output of some system with some unknown input u_n. Such models are expressed as the following relation,

$$s_n = -\sum_{k=1}^{p} a_k s_{n-k} + G\sum_{l=0}^{q} b_l u_{n-l}, \quad b_0 = 1, \tag{4.3}$$

where a_k, $1 \le k \le p$, b_l, $1 \le l \le q$ are called predictor coefficient and G is the gain of the hypothesized system. The output s_n is shown as a linear combination of past outputs, present and past inputs in (4.3). The method for predicting s_n by using (4.3) is called linear prediction. Therefore, the object of linear prediction is to estimate the output sequence from a linear combination of input samples, past samples or both.

The linear prediction can be converted in the frequency domain by taking the z transform on (4.3). Then the transfer function $H(z)$ of the system is a ratio of polynomials $S(z)$ and $U(z)$, and is followed as

$$H(z) = \frac{S(z)}{U(z)} = G\frac{1+\sum_{l=1}^{q} b_l z^{-l}}{1+\sum_{k=1}^{p} a_k z^{-k}}, \tag{4.4}$$

where

$$S(z) = \sum_{n=-\infty}^{\infty} s_n z^{-n} \tag{4.5}$$

is the z transform of s_n and $U(z)$ is the z transform of u_n. In (4.4), the roots of the numerator and denominator polynomials are the zeros and poles of the model, respectively. Hence, $H(z)$ is the general pole-zero model.

The pole-zero model can be divided into two cases. The two cases are as follows.

1) all-zero model: $a_k = 0, \quad 1 \le k \le p$
2) all-pole model: $b_l = 0, \quad 1 \le l \le q$

In statistics, all-zero model is known as the moving average (MA) model and all-pole model is known as the autoregressive (AR) model [18]. The denominator $U(z)$ is equal to unity in all-zero model and the numerator $S(z)$ is constant in the all-poll model. The mixed pole-zero model is also known as the autoregressive moving average (ARMA) model.

In this dissertation, it is focused on the all-pole model. In the all-pole model, a signal s_n can be expressed as a linear combination of past samples and some input sample u_n due to $b_l = 0, \quad 1 \le l \le q$,

$$s_n = -\sum_{k=1}^{p} a_k s_{n-k} + G u_n, \tag{4.6}$$

where G is a gain factor. This model in the time domain is shown as Figure 4.19.

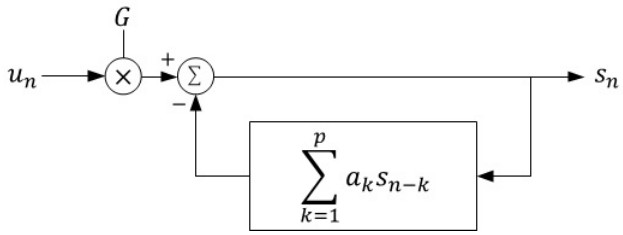

Figure 4.19 The all-pole model in the time domain

The transfer function $H(z)$ can be reduced as follow,

$$H(z) = \frac{G}{1 + \sum_{k=1}^{p} a_k z^{-k}}. \tag{4.7}$$

The all-pole model in the frequency domain is shown as Figure 4.20.

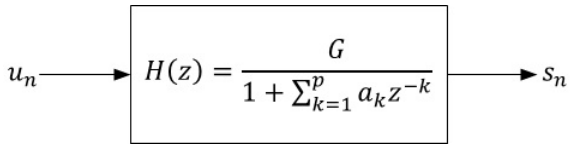

Figure 4.20 The all-pole model in the frequency domain

Now, the problem is to determine the predictor coefficients a_k and the gain G, given a certain signal s_n. The derivation of coefficients a_k will be given by using least square (LS) method assuming that the signal s_n is a deterministic signal and the input u_n is unknown. Then, the signal s_n can be approximately predicted from a linear summation of past samples. The

approximation of s_n is expressed as

$$\widetilde{s_n} = -\sum_{k=1}^{p} a_k s_{n-k} \ . \tag{4.8}$$

Then, the error of the real value s_n and the predicted value $\widetilde{s_n}$ is represented by

$$e_n = s_n - \widetilde{s_n} = s_n + \sum_{k=1}^{p} a_k s_{n-k} \ . \tag{4.9}$$

The coefficients a_k are calculated by minimizing the total squared error with each of the parameters. The total squared error E is expressed as

$$E = \sum_n e_n^2 = \sum_n \left(s_n + \sum_{k=1}^{p} a_k s_{n-k} \right)^2 \ . \tag{4.10}$$

The total squared error can be minimized by setting

$$\frac{\partial E}{\partial a_i} = 0, \quad 1 \le i \le p \ . \tag{4.11}$$

By substituting (4.10) in (4.11), the following equation can be obtained,

$$\sum_{k=1}^{p} a_k \sum_{n} s_{n-k} s_{n-i} = -\sum_{n} s_n s_{n-i}, \quad 1 \le i \le p. \tag{4.12}$$

Because that equation (4.12) is composed of p equations with p unknowns, the equation can be solved for predictor coefficients which minimize the total squared error.

By expanding (4.10) and substituting (4.12), the minimum total squared error $E_{\min}$ is obtained as

$$E_{\min} = \sum_{n} s_n^2 + \sum_{k=1}^{p} a_k \sum_{n} s_n s_{n-k} . \tag{4.13}$$

Let the range of summation over n in (4.10) specify the infinite duration $-\infty < n < \infty$. Then the equation (4.12) can be reduced to

$$\sum_{k=1}^{p} a_k R(i-k) = -R(i), \quad 1 \le i \le p \tag{4.14}$$

and the equation (4.13) can be also reduced to

$$E_{\min} = R(0) + \sum_{k=1}^{p} a_k R(k) \tag{4.15}$$

where

$$R(i) = \sum_{n=-\infty}^{\infty} s_n s_{n+i} \tag{4.16}$$

is the autocorrelation function of the signal s_n. As $R(i)$ is an even function of i, the following relation holds

$$R(i) = R(-i). \tag{4.17}$$

Then the autocorrelation matrix is a symmetric Toeplitz matrix [37]. Therefore, equation (4.14) can be expressed in a matrix form as

$$\begin{bmatrix} R_0 & R_1 & R_2 & \cdots & R_{p-1} \\ R_1 & R_0 & R_1 & \cdots & R_{p-2} \\ R_2 & R_1 & R_0 & \cdots & R_{p-3} \\ \vdots & \vdots & \vdots & \ddots & \vdots \\ R_{p-1} & R_{p-2} & R_{p-3} & \cdots & R_0 \end{bmatrix} \begin{bmatrix} a_1 \\ a_2 \\ a_3 \\ \vdots \\ a_p \end{bmatrix} = - \begin{bmatrix} R_1 \\ R_2 \\ R_3 \\ \vdots \\ R_p \end{bmatrix}. \tag{4.18}$$

The solution of (4.18) is obtained by using Burg's method [38]. The burg's method estimates the reflection coefficients and uses the reflection coefficients to estimate the AR coefficient parameters recursively. It is found that the recursion and lattice filter relations describing the update of the forward and backward prediction errors in [39].

4.3.2 Linear Prediction for the Sum of Sinusoids

In the section 3 of Chapter 2, the mixer signal is expressed by

$$m_S(t) = \sum_{i=1}^{M} C_i \cos\left(2\pi\left(\frac{BW}{\Delta t} t_{d,i} - f_{d,i} \right) t + 2\pi\left(f_c - \frac{BW}{2} + f_{d,i} \right) t_{d,i} - \frac{\pi BW}{\Delta t} t_{d,i}^2 \right)$$

. (4.19)

The mixer signal is the sum of M sinusoids. It is well known that a sample of the sum of M sinusoids at time nT can be uniquely represented as a linear combination of at least the past $2M$ samples at times $(n-1)T, \cdots, (n-2M)T$ [20]. For proof, a sample of the mixer signal $m_s(n)$ is simply re-expressed as

$$m_S(n) = \sum_{i=1}^{M} C_i \sin(\omega_i n + \phi_i). \quad (4.20)$$

If a unique $2M$ vector exists $\mathbf{a}^T = [a_1, a_2, \cdots, a_{2M}]$, a sample of mixer signal can be expressed as

$$\begin{aligned} m_S(n) &= \sum_{k=1}^{2M} a_k \sum_{i=1}^{M} C_i \sin(\omega_i (n-k) + \phi_i) \\ &= \sum_{k=1}^{2M} a_k m_S(n-k) \end{aligned} \quad . \quad (4.21)$$

Using the formula of the sine function, (4.21) can be re-expressed as

$$m_S(n) = \sum_{i=1}^{M} C_i \sin(\omega_i n + \phi_i) \sum_{k=1}^{2M} a_k \cos \omega_i k - \sum_{i=1}^{M} C_i \cos(\omega_i n + \phi_i) \sum_{k=1}^{2M} a_k \sin \omega_i k \ . \tag{4.22}$$

Since (4.20) and (4.22) are equal for all i, following equations are satisfied as for $i = 1, 2, \cdots, M$,

$$\sum_{k=1}^{2M} a_k \cos \omega_i k = 1 \tag{4.23}$$

and

$$\sum_{k=1}^{2M} a_k \sin \omega_i k = 0 \, . \tag{4.24}$$

Combining (4.23) and (4.24) , matrix form is as follows,

$$F\mathbf{a} = \mathbf{q} \tag{4.25}$$

where

$$F = \begin{bmatrix} \cos\omega_1 & \cdots & \cos 2\mathrm{M}\,\omega_1 \\ \vdots & & \vdots \\ \cos\omega_M & \cdots & \cos 2M\,\omega_M \\ \sin\omega_1 & \cdots & \sin 2M\,\omega_1 \\ \vdots & & \vdots \\ \sin\omega_M & \cdots & \sin 2M\,\omega_M \end{bmatrix} \tag{4.26}$$

and

$$\mathbf{q}^T = \begin{bmatrix} 1 & \cdots & 1 & 0 & \cdots & 0 \end{bmatrix}. \tag{4.27}$$

If F^{-1} exists, a is unique. Consider following matrix, with $\lambda_i = e^{j\omega_i}$, given by

$$B = \begin{bmatrix} D^* & D \\ jD^* & -jD \end{bmatrix}, \tag{4.28}$$

where $D = diag\left(\lambda_1, \cdots, \lambda_M\right)$. Then, it may be seen that

$$\begin{aligned} V &= F^T B \\ &= \begin{bmatrix} 1 & \cdots & 1 & 1 & \cdots & 1 \\ \lambda_1 & \cdots & \lambda_M & \lambda_1^* & \cdots & \lambda_M^* \\ \lambda_1^2 & \cdots & \lambda_M^2 & \lambda_1^{*2} & \cdots & \lambda_M^{*2} \\ \vdots & & \vdots & \vdots & & \vdots \\ \lambda_1^{2M-1} & \cdots & \lambda_M^{2M-1} & \lambda_1^{*2M-1} & \cdots & \lambda_M^{*2M-1} \end{bmatrix}. \end{aligned} \tag{4.29}$$

The matrix V in (4.29) is the nonsingular Vandermonde matrix [40]. It is

easy to see that $|B| \neq 0$ and therefore $|F| \neq 0$. Hence, it is proved that a unique a which satisfies (4.21) exists. A vector a can be obtained by solving (4.18).

4.3.3 Proposed Algorithm using Linear Prediction

In the previous subsection (4.2.2), it is seen that a sample of the sum of sinusoids can be expressed as a linear combination of past samples. Therefore, AR model can be applied to the mixer signal which is represented by the sum of sinusoids.

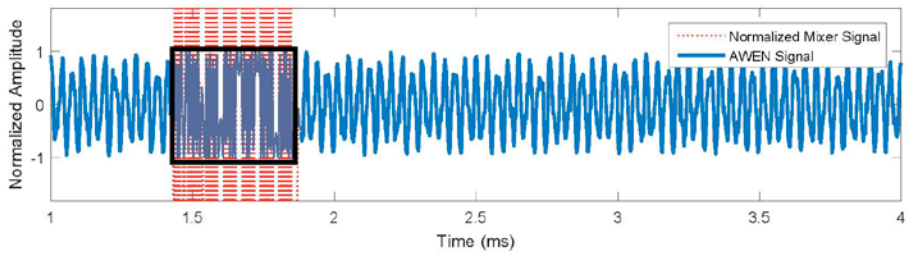

Figure 4.21 AWEN signal (case3)

For simulation, the scenario which is shown as right side in Figure 3.9 is assumed. The interference signal is generated in relative long time (case3). In Figure 4.21, blue solid line is AWEN signal which the interference is suppressed. The signal in the black box is still distorted compared to both side of black box, because that only amplitude of interference is suppressed. The partial portion corresponding the black box is considered as “the missing

region".

The first step to restore signal in the missing region is to calculate the prediction coefficient a_k of the AWEN signal. In the second step, the data in the missing region are predicted by using forward prediction from the left side of the missing region and backward prediction from the right side. Consider the situation which the missing region is leaned to one side.

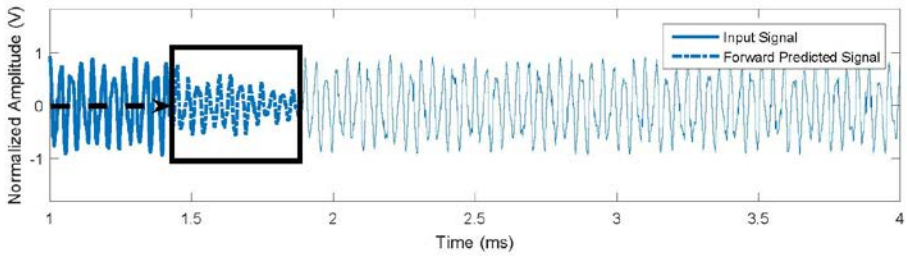

Figure 4.22 Forward prediction

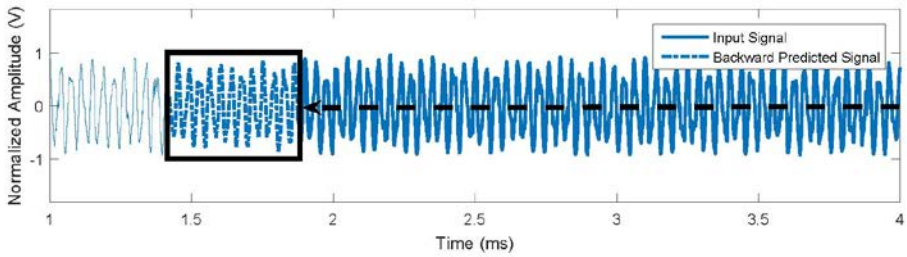

Figure 4.23 Backward prediction

The results of prediction from both side of the missing region are shown in the black box in Figure 4.22 and 23. The bold line signal is input data of predictor and the dotted arrow indicates the direction of prediction. To

compute restored signal $\widehat{m}_S(n)$ given the two predicted signals $\widehat{m}_F(n)$ and $\widehat{m}_B(n)$, the two predicted signals are crossfaded by multiplying $\widehat{m}_F(n)$ by the window function $w(n)$ and $\widehat{m}_B(n)$ by $1-w(n)$,

$$\widehat{m}_S(n) = w(n)\widehat{m}_F(n) + (1-w(n))\widehat{m}_B(n). \tag{4.30}$$

As shown in Figure 4.22 and 23, the result of backward prediction is more quality than the one of the forward prediction, because that the length of input data for backward prediction l_B is longer than the one for forward prediction l_F. Therefore, the window $w(n)$ which is used to crossfade the two predicted signal should be asymmetric to be weighted in favor of the longer signal. The symmetric cosine window is computed by

$$w(n) = \frac{1}{2}\left(1+\cos\left(\pi\left(1+\frac{n}{L}\right)\right)\right), \quad 0 \le n \le L, \tag{4.31}$$

where L is the length of the missing region. The window $w(n)$ has values of 0, 0.5 and 1 when $n=0$, $n=\frac{L}{2}$ and $n=L$, respectively. Now, the asymmetric window function $w_{asy}(n)$ can be made by using the symmetric window function $w(n)$ under the following constraint,

$$w_{asy}\left(\frac{l_F}{l_F+l_B}L\right)=\frac{1}{2}. \tag{4.32}$$

Consider new variable n' in place of n. The relationship between n and n', $n'=f(n)$ should satisfy the given conditions,

1) $0=f(0)$
2) $L=f(L)$
3) $\frac{L}{2}=f\left(\frac{l_F}{l_F+l_B}L\right)$.

Also, f should be monotonically increasing function. Hence, the following function (4.33) is considered,

$$n'=\frac{b}{n+a}+c\,. \tag{4.33}$$

Given three conditions, three variables can be solved. Then, the asymmetric window function is given by

$$w_{asy}(n)=w\left(\frac{b}{n+a}+c\right),\quad 0\le n\le L\,. \tag{4.34}$$

The proposed asymmetric window is shown in Figure 4.24. The symmetric window function is used if $l_F=l_B$ and the asymmetric window function is

used if $l_F \neq l_B$.

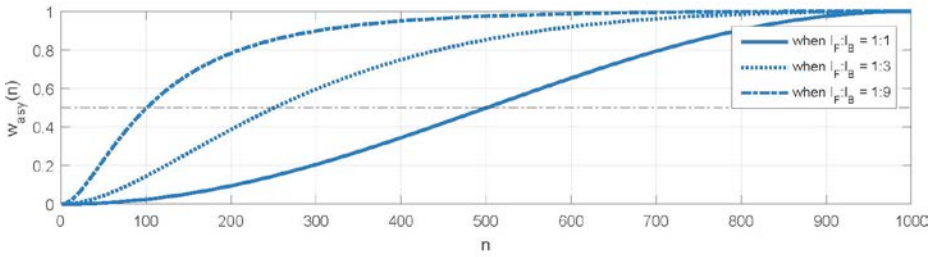

Figure 4.24 The asymmetric window

The power factor also should be considered only if the order of linear prediction p is smaller than l_F or l_B. The power factor is computed according to l_F and l_B,

$$c(l) = \frac{\sqrt{\sum_{k=1}^{p} a_k^2}}{\sqrt{\sum_{2}^{\min(p,l)} a_k^2}}. \tag{4.35}$$

Finally, the restored signal $\hat{m}_S(n)$ can be asymmetrically crossfaded to given two predicted signals,

$$\hat{m}_S(n) = c(l_F)\, w_{asy}(n)\, \hat{m}_F(n) + c(l_B)\, w_{asy}\, \hat{m}_B(n). \tag{4.36}$$

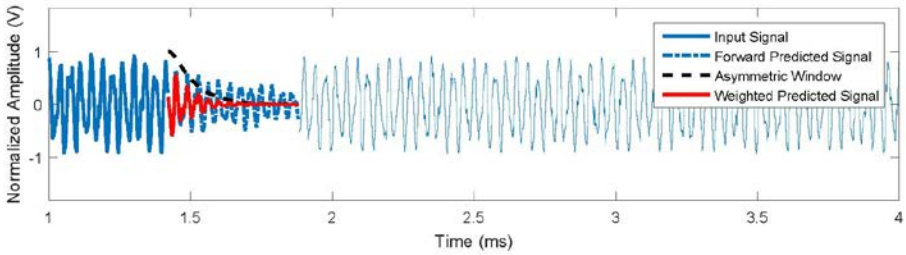

Figure 4.25 Forward prediction with the proposed window (case3)

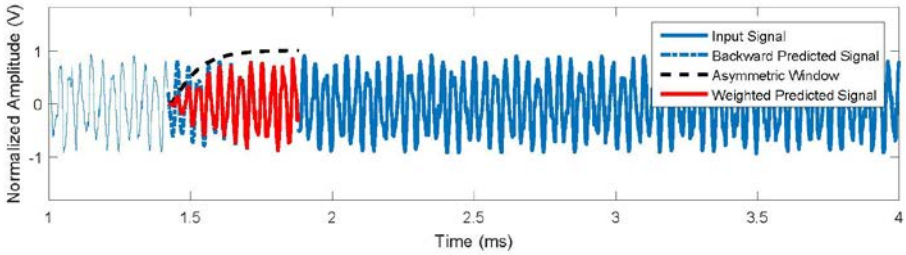

Figure 4.26 Backward prediction with the proposed window (case3)

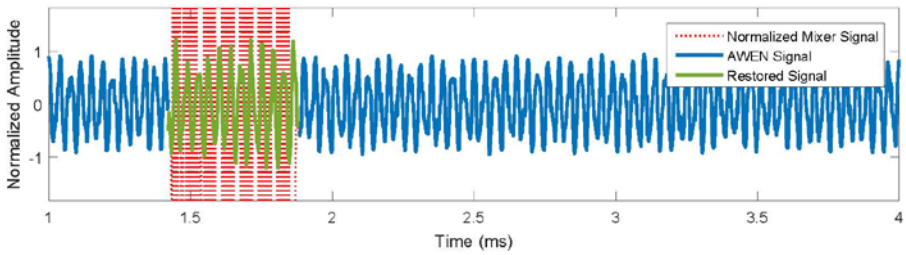

Figure 4.27 The result of prediction with asymmetric crossfading (case3)

The processes of asymmetric crossfading are depicted in Figure 4.25 and 26. Because that the missing region is leaned to left side, the length for forward prediction l_F is shorter than the one for backward prediction l_B. As shown

in Figure 4.25, the predicted signal follows the tendency, but the amplitude is relatively reduced. To weight the predicted signal from backward prediction, the asymmetric window is used. The asymmetric window is black dotted line and the result of crossfading is red line. Then, the correctly restored signal is shown as green line in Figure 4.27. Compared to both side of missing region, it is seen that the restored signal is naturally connected. Without meaning to, the noise level of restored signal spectrum is lowered a little than the one of AWEN signal spectrum as shown in Figure 4.28. Since the noise level is lowered more than 20 dB from AWEN and restoration, target SNR is increased more than 30 dB and then target peak can very stably detected. Since multiple rectangular is multiplied to the mixer signal in the time domain, comb-shape frequency response is obtained. By restored, comb-shape response is removed and then the noise floor is lowered.

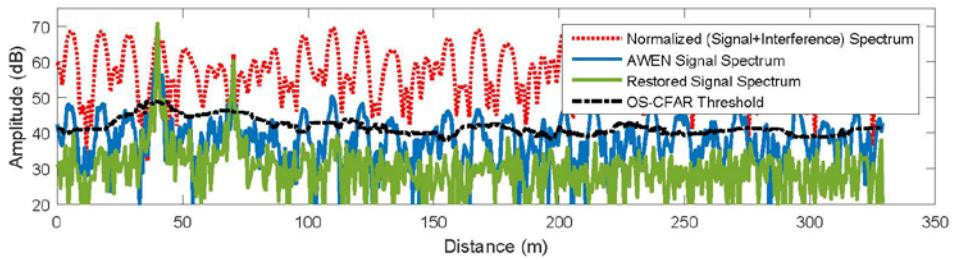

Figure 4.28 Spectrum of the restored signal (case3)

The pseudo spectrum of MUSIC which was the motivation for restoration is shown in Figure 4.29.

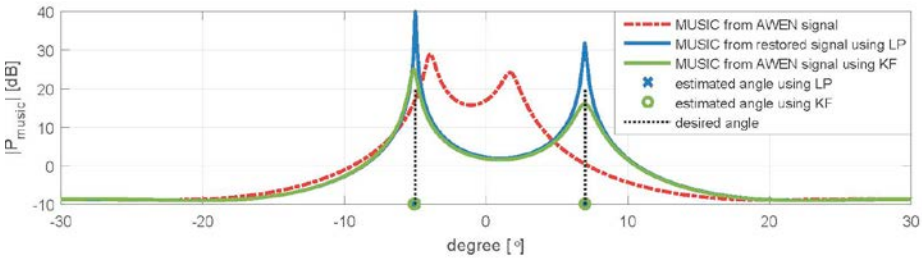

Figure 4.29 Pseudo spectrum of MUSIC for restored signal (case3)

The red dotted line is the spectrum from AWEN signal shown in the early section. From the MUSIC pseudo spectrum of the proposed restored signal, it is seen that estimated angles are almost the same as the desired angles. Also it is depicted the result of Kalman filter using prediction coefficients a_k from (4.18) based on AR model. The numerical expression (4.21) is used for the state model of Kalman filter. When the missing region, Kalman gain is set to about zero and the predicted value is not corrected by measurement data. The estimated angle accuracy was evaluated about case3 using the root mean square error (RMSE) as shown in Table 4.1.

Table 4.2 RMSE performance of MUSIC

Iteration : 1000	Linear prediction	Kalman filter
RMSE	0.0268°	0.0219°

Since the same signal model is used in prediction, the difference of RMSE performance between the proposed method and Kalman filter is almost same,

and the values are very small. Therefore, it is seen that the signal prediction based on AR model is useful for angle estimation.

4.4 Conclusion

In this chapter, we proposed an advanced weighted-envelope normalization algorithm in the time domain in order to minimize the effects of interference. AWEN algorithm is resulted from the characteristic of the impulse-like interference between FMCW radars. From simulation results, we verified that the proposed AWEN algorithm can detect the targets despite of severe transient interference environments. While the performance of conventional algorithms highly depends on the SIR, the proposed algorithm is shown to be resilient to low SIR condition with multiple interference sources. The proposed algorithm has been verified from the measurement. The detection probability is improved and the false alarm rate of the FMCW radar is reduced by applying simple signal processing method.

After suppressing the interference signal in the time domain, accurate range and velocity can be calculated, but angle of target cannot be correctly estimated. The method for restoring the distorted signal by using linear prediction is proposed. In order to effectively restore the signal, the asymmetric window function is suggested from simulation result. Since the partial portion which the interference is suppressed is restored, angle of target is accurately estimated from MUSIC.

Finally, by applying interference suppression algorithm and signal restoration method to the mixer signal with interference, correct angle as well as range and velocity can be estimated in automotive FMCW radar.

Bibliography

[1] I. Gresham, N. Jain, T. Budka, A. Alexanian, N. Kinayman, B. Ziegner, S. Brown, and P. Staecker, "A 76-77 GHz pulsed-doppler radar module for autonomous cruise control applications," *Microwave Symposium Digest. 2000 IEEE MTT-S International*, pp.1551–1554, IEEE, 2000.

[2] K. Lukin, A. Mogyla, Y.A. Alexandrov, O. Zemlyaniy, T. Lukina,and Y. Shiyan, "W-band noise radar sensor for car collision warning systems," *Physics and Engineering of Millimeter and Sub-Millimeter Waves, 2001. The Fourth International Kharkov Symposium on*, pp.870–872, IEEE, 2001.

[3] A.G. Stove, "Linear FMCW radar techniques," *IEE Proceedings F (Radar and Signal Processing)*, pp.343–350, IET, 1992.

[4] H. Rohling and M.M. Meinecke, "Waveform design principles for automotive radar systems," Radar, *2001 CIE International Conference on, Proceedings*, pp.1–4, IEEE, 2001.

[5] S.H. Jeong, J.N. Oh, and K.H. Lee, "Design of 24 GHz radar with subspace-based digital beam forming for ACC Stop-and-Go system," *ETRI journal*, vol.32, no.5, 2010.

[6] M. Schneider, "Automotive radar–status and trends," *German microwave conference*, pp.144–147, 2005.

[7] G.M. Brooker, "Mutual interference of millimeter-wave radar systems," *Electromagnetic Compatibility, IEEE Transactions on*, vol.49, no.1, pp.170–181, 2007.

[8] M. Goppelt, H.L. Blocher, and W. Menzel, "Automotive radar investigation of mutual interference mechanisms.," *Advances in Radio Science*, vol.8, 2010.

[9] M. Goppelt, H.L. Blocher, andW. Menzel, "Analytical investigation of mutual interference between automotive fmcw radar sensors," *Microwave*

Conference (GeMIC), 2011 German, pp.1–4, IEEE, 2011.

[10] SIEMENS AG, “Microwave reflector aerial for car distance warning radar”, Oct. 19 1995. DE Patent 4412769

[11] V. Filimon and J. Buechler, “A pre-crash radar sensor system based on pseudo-noise coding,” *Microwave Symposium Digest. 2000 IEEE MTT-S International*, pp.1415–1418, IEEE, 2000.

[12] J.H. Zhang, G.S. Liu, H. Gu, and W.M. Su, “A novel transmit signal based on high range-resolution concept for flar or aicc system applications,” *CIE International Conference on Radar (2001: Beijing, China). Proceedings*, 2001.

[13] B.E. Tullsson, “Topics in fmcw radar disturbance suppression,” 1997.

[14] H. Gokalp, G. Taflan, and S. Salous, “In-band interference reduction in fmcw channel data using prony modelling,” *Electronics Letters*, vol.45, no.2, pp.132–133, 2009.

[15] L. Mu, T. Xiangqian, S. Ming, and Y. Jun, “Research on key technologies for collision avoidance automotive radar,” *Intelligent Vehicles Symposium*, 2009 IEEE, pp.233–236, IEEE, 2009.

[16] Sakkila, L., et al. "Short range automotive radar based on UWB pseudo-random coding." *Telecommunications, 2007. ITST'07. 7th International Conference on ITS*. IEEE, 2007.

[17] W. Szajnowski, “Automotive radar with composite multi-slope fm chirp waveform,” Feb. 4 2010. WO Patent App.PCT/EP2009/059,862.

[18] Anderson, Theodore Wilbur. *The statistical analysis of time series*. Vol. 19. John Wiley & Sons, 2011.

[19] Bartlett, Maurice Stevenson. *An introduction to stochastic processes, with special reference to methods and applications*. CUP Archive, 1978.

[20] Box, George EP, Gwilym M. Jenkins, and Gregory C. Reinsel. *Time series analysis: forecasting and control*. Vol. 734. John Wiley & Sons, 2011.

[21] Makhoul, John. "Linear prediction: A tutorial review." *Proceedings of the*

*IEEE*63.4 (1975): 561-580.

[22] Chan, Y. T., J. Lavoie, and J. B. Plant. "A parameter estimation approach to estimation of frequencies of sinusoids." *Acoustics, Speech and Signal Processing, IEEE Transactions on* 29.2 (1981): 214-219.

[23] Axelsson, Sune RJ. "Area target response of triangularly frequency-modulated continuous-wave radars." *Aerospace and Electronic Systems, IEEE Transactions on* 2 (1978): 266-277.

[24] Barrick, D. E., and E. Bahar. "Rough surface scattering using specular point theory." *Antennas and Propagation, IEEE Transactions on* 29.5 (1981): 798-800.

[25] Tozzi, Louis Mario. *Resolution in frequency-modulated radars*. University of Maryland., 1972.

[26] Skolnik, Merrill I. "Introduction to radar." *Radar Handbook* 2 (1962).

[27] Minkler, Gary, and Jing Minkler. "CFAR: the principles of automatic radar detection in clutter." *NASA STI/Recon Technical Report A* 90 (1990): 23371.

[28] Rohling, Hermann. "Radar CFAR thresholding in clutter and multiple target situations." *Aerospace and Electronic Systems, IEEE Transactions on* 4 (1983): 608-621.

[29] Rohling, H. "Some radar topics: waveform design, range CFAR and target recognition." *Advances in Sensing with Security Applications*. Springer Netherlands, 2006. 293-322.

[30] Levanon, Nadav. "Detection loss due to interfering targets in ordered statistics CFAR." *IEEE Transactions on Aerospace Electronic Systems* 24 (1988): 678-681.

[31] Bartlett, MAURICE STEVENSON. "Smoothing periodograms from time series with continuous spectra." *Nature* 161.4096 (1948): 686-687.

[32] Capon, Jack. "High-resolution frequency-wavenumber spectrum analysis."*Proceedings of the IEEE* 57.8 (1969): 1408-1418.

[33] Schmidt, Ralph O. "Multiple emitter location and signal parameter

estimation."*Antennas and Propagation, IEEE Transactions on* 34.3 (1986): 276-280.

[34] Norden, R. H. "A survey of maximum likelihood estimation." *International Statistical Review/Revue Internationale de Statistique* (1972): 329-354.

[35] Norden, R. H. "A survey of maximum likelihood estimation: Part 2."*International Statistical Review/Revue Internationale de Statistique* (1973): 39-58.

[36] Paulraj, Arogyaswami, Richard Roy, and Thomas Kailath. "Estimation of signal parameters via rotational invariance techniques-ESPRIT." *Circuits, Systems and Computers, 1985. Nineteeth Asilomar Conference on*. IEEE, 1985.

[37] Grenander, Ulf, and Gabor Szegö. *Toeplitz forms and their applications*. Vol. 321. Univ of California Press, 1958.

[38] Burg, John Parker. "Maximum entropy spectral analysis." *37th Annual International Meeting.*. Society of Exploration Geophysics, 1967.

[39] Kay, Steven M. *Modern spectral estimation*. Pearson Education India, 1988.

[40] Ogata, Katsuhiko. *State space analysis of control systems*. Prentice-Hall, 1967.

초록

도로 위에 자동차의 수가 늘어남에 따라 교통사고가 점차 증가하고, 사망자 또한 많아지고 있다. 만일 자동차가 능동적으로 위험상황을 인지하고 운전자에게 경고를 할 수 있다면, 운전자에게 매우 유용할 것이다. 이에 많은 자동차 제조사와 차량용 부품 제조사들은 센서 기술들을 개발해오고 있다. 자동차용 센서에는 카메라, LIDAR, 레이더 그리고 초음파 등이 있다. 이들 센서들 중, 레이더가 자동 주행 시스템에 있어서 가장 중요한 부품으로 사용되고 있다. 레이더는 날씨나 밤낮을 가리지 않고 뛰어난 성능을 보이는 반면, 카메라는 밤이나 비가 오는 경우에 성능 저하가 일어나고, LIDAR는 아직 상용화하기에는 높은 비용이 발생하며, 초음파는 매우 짧은 거리에서만 사용된다.

레이더 센서에는 펄스 도플러 레이더, SFPD 레이더, FMCW 레이더 그리고 랜덤 잡음 레이더 등이 있다. 펄스 도플러 레이더나 랜덤 잡음 레이더는 높은 해상도를 위한 고성능의 하드웨어가 필요하고 SFDP 레이더는 추가적인 신호 처리 기법이 필요하지만, FMCW 레이더는 높은 해상도와 구현하기 쉬운 이점으로 인해 차량용 레이더로 주로 사용된다.

레이더를 장착한 차량이 늘어남에 따라, 레이더는 목표물뿐만 아니라 다른 레이더로부터 신호를 받게 된다. 간섭 신호는 심각한 문제를 초래한다. 레이더의 오작동을 방지하기 위해, 간섭으로 인한 영향을 제거해야 한다. 간섭 제거 기법으로 신호 처리하기 전에

직접 간섭 신호를 제거하는 방법 그리고 신호 처리 후에 간섭으로 인한 영향을 제거하는 방법 등이 연구되고 있다.

본 논문에서는 FMCW 레이더간의 간섭의 영향에 대해 분석하였다. 먼저 동일한 레이더나 chirp 신호의 기울기가 조금 다른 레이더에서 협대역 비트 주파수로 인해 발생하는 고스트 목표물 같은 현상이 일어난다. 간섭의 대부분은 광대역 비트 주파수로 인해 주파수 도메인에서 잡음 레벨이 올라가는 현상이 일어난다. 이러한 광대역 비트 주파수를 가지는 간섭 신호는 제한되는 대역폭으로 인해 임펄스와 같은 모양을 가진다. 간섭 신호는 시간 영역에서 그들의 포락선을 이용하여 제거할 수 있다. 이러한 방법의 효과는 시뮬레이션 결과와 무반향실에서 측정한 데이터를 통해 확인한다.

시간 영역에서 간섭 신호가 제거되었음에도, 여전히 간섭의 흔적이 남아있다. 이러한 이유로 정확한 각도 추정이 이루어지지 않는다. FMCW 레이더의 신호는 사인 곡선의 합으로 이루어져 있기 때문에 선형 예측 기법을 통해 간섭의 흔적을 새로운 신호로 복원할 수 있다. 또한, 더 정확한 예측을 하기 위해 비대칭 윈도우 함수를 제안하고 이를 이용하여 정방향으로 예측한 신호와 역방향으로 예측한 신호를 크로스페이딩한다. 이 방법의 효과 또한 시뮬레이션 결과를 통해 확인한다.

주요어 : FMCW, 간섭, 억제, 선형 예측, 자기 회기 모델, 신호 복원
학　번 : 2010 – 30234